

Topi Rasku

# **Energy Management in Households with Coupled Photovoltaics and Electric Vehicles**

**School of Science**

Thesis submitted for examination for the degree of Master of Science in  
Technology

Espoo September 29, 2015

**Thesis Supervisor:**

Prof. Peter Lund

**Thesis Advisors:**

M.Sc. (Tech.) Jyri Salpakari

M.Sc. (Tech.) Juuso Lindgren

Author: Topi Rasku

Title: Energy Management in Households with Coupled Photovoltaics and Electric Vehicles

Date: September 29, 2015      Language: English      Pages: 64+2

Department of Applied Physics

Professorship: Tfy-56 Advanced Energy Systems

Supervisor: Prof. Peter Lund

Advisors: M.Sc. (Tech.) Jyri Salpakari, M.Sc. (Tech.) Juuso Lindgren

With the increasing penetration of distributed renewable energy generation, time-of-use and real-time electricity pricing, as well as plug-in electric vehicles, applications for residential demand side management are becoming more appealing. In this work, we study the economical benefits of vehicle-to-grid and space heating load control for residential consumers with local photovoltaic generation. A linear programming model is constructed for cost-optimizing the energy management of multiple households with various electric vehicle and space heating system combinations, resulting in yearly electricity cost savings between €120–290 (14–40%) per household. The benefits of increasing the number of co-operating households are found to saturate around 5 households, and we also highlight the importance of accounting for battery degradation costs in vehicle-to-grid optimization.

Keywords: Energy management, electric vehicles, vehicle-to-grid, photovoltaics, space heating load control, linear programming

Tekijä: Topi Rasku

Työn nimi: Kotitalouksien energianhallinta aurinkosähköä ja sähköautoja hyödyntäen

Päivämäärä: 29.9.2015

Kieli: Englanti

Sivumäärä: 64+2

Teknillisen fysiikan laitos

Professuuri: Tfy-56 Energiateetet

Työn valvoja: Prof. Peter Lund

Työn ohjaajat: DI Jyri Salpakari, DI Juuso Lindgren

Hajautettujen uusiutuvien energianlähteiden, sähkön yö- ja tunneittaisen hinnoittelun, sekä sähköautojen yleistymisen myötä kysyntäjouaston sovellukset kotitalouksilla ovat käyneet yhä houkuttelevammiksi. Tässä työssä tarkastellaan *vehicle-to-grid* -tekniikan ja lämmitysjouaston taloudellista hyötyä aurinkosähkön pientuottajille, sekä muodostetaan lineaariseen optimointiin pohjautuva usean kotitalouden kustannusoptimaalinen energianhallintamalli. Saavutetut optimaaliset vuosittaiset kustannussäästöt yksittäisille kotitalouksille vaihtelevat noin 120–290 euron (14–40%) välillä, riippuen mallinnetuista sähköautoista ja lämmitysjärjestelmistä. Kotitalouksien määrän lisäämisen hyödyn havaitaan saavuttavan maksiminsa jo viiden kotitalouden kohdalla, ja tuloksista käy ilmi akkujen kulumisen kustannusten mallintamisen tärkeä rooli *vehicle-to-grid* ohjauksen optimoinnissa.

Avainsanat: Energianhallinta, sähköautot, *vehicle-to-grid*, aurinkosähkö, lämmitysjousto, lineaarinen optimointi

## Contents

Abstract . . . . .	ii
Abstract (in Finnish) . . . . .	iii
Symbols and Abbreviations . . . . .	v
<b>1. Introduction</b>	<b>1</b>
<b>2. Background</b>	<b>4</b>
2.1 Space Heating Load Control . . . . .	4
2.2 PEV Smart Charging and Vehicle-to-Grid . . . . .	6
2.3 Battery Management Systems and Battery Ageing . . . . .	8
<b>3. Data and Modelling</b>	<b>11</b>
3.1 PEV Availability and Movement . . . . .	12
3.2 PEV Batteries and Thermal Management . . . . .	18
3.3 Space Heating Load . . . . .	28
3.4 Renewable Generation and Energy Prices . . . . .	36
<b>4. Linear Programming Formulation</b>	<b>38</b>
4.1 PEV Battery Constraints . . . . .	38
4.2 House HVAC Constraints . . . . .	42
4.3 Microgrid Power Balance and Objective Functions . . . . .	44
<b>5. Results and Discussion</b>	<b>47</b>
5.1 Model Validation . . . . .	48
5.2 Individual Households . . . . .	52
5.3 Microgrid Size . . . . .	54
5.4 Photovoltaic Generation . . . . .	57
5.5 PEV Infrastructure . . . . .	58
<b>6. Summary and Conclusions</b>	<b>61</b>
<b>Bibliography</b>	<b>65</b>
<b>A. Linear Differential Equation System</b>	<b>71</b>

## Symbols and Abbreviations

### Symbols

<b>A</b>	Initial vehicle thermal coefficient matrix
$A_{p,h}$	Estimated surface area of structural part $p$ of house $h$
$a_c$	Battery ageing model coefficient
<b>B<sub>h</sub></b>	Initial house $h$ thermal coefficient matrix
<b>b<sub>t</sub></b>	Vehicle thermal model vector on time $t$
$b$	Battery ageing model fitting parameter
$C_{n,h}$	Heat capacity of node $n$ for house $h$
$C_{ref}$	<i>TABULA</i> reference heat capacity
<b>c<sub>h,t</sub></b>	House $h$ thermal model vector on hour $t$
$c_{dhw}$	Specific heat capacity of water at 60°C
$c_{in}$	Specific heat capacity of water at 8°C
$c_a$	Volumetric specific heat capacity of air at 20°C
$c_c$	Volumetric specific heat capacity of concrete
$c$	Battery ageing model fitting parameter
$D_{v,t}^-$	Driving energy consumption of vehicle $v$ on hour $t$
<b>d<sub>1/2</sub></b>	Vector determining the inequality (1) or equality (2) constraints of a LP problem
$E_{max,v,0}$	Nominal battery capacity of vehicle $v$
$E_{v,t}$	Energy stored in the battery of vehicle $v$ on hour $t$
$E_{ac}$	Cell activation energy for the capacity fade process
$F_{max,v}^+$	Maximum fuel charging power of vehicle $v$
$F_{v,t}^+$	Fuel charging power of vehicle $v$ on hour $t$
<b>f</b>	Vector containing the coefficients of the objective function of a LP problem
$f_j(t)$	Probability density for type $j$ journey as a function of hour $t$
$f_{obj}$	Objective function for <i>obj</i> optimization
$G_{v,t}^{+/-}$	Electric power directly charged (+) to or discharged from (-) the electricity market of vehicle $v$ on hour $t$
$G_{s/b,t}$	Electricity sold ( $s$ ) to and bought ( $b$ ) from the market to the home grid on hour $t$
$G_{max}$	Maximum electricity traded by home grid
$g_{v,t}$	Vehicle $v$ grid-connection binary on hour $t$
$H_{nm,(h)}$	Heat transfer coefficient between nodes $n$ and $m$ (of house $h$ )

$H_{dhw}$	Heat transfer coefficient between the domestic hot water storage tank and the ambient air
$h_{wa}$	Minimum residential dwelling room height
$h_v$	Vehicle $v$ plug-in hybrid binary
$I$	Total current through the battery
$I_{sol,t}$	Solar irradiance on hour $t$
$J_t$	Ampere-hour throughput of the whole battery system
$\hat{j}_t$	Ampere-hour throughput of a single battery cell
$L_{v,t}$	Battery capacity loss percentage of vehicle $v$ at hour $t$
$\mathbf{M}_{1/2}$	Matrix determining the inequality (1) or equality (2) constraints of a LP problem
$N_{ppl,h}$	Number of residents in house $h$
$N_h$	Number of modelled households
$N_{Y/N}$	Number of people who either travelled ( $Y$ ) or didn't ( $N$ ) on their day of survey
$P_{v,t}^{+/-}$	Electric power charged (+) to and discharged (-) from vehicle $v$ on hour $t$
$P_{h,t}^{+/-}$	Electric power draw of the heating (+) and cooling (-) equipment of house $h$ on hour $t$
$P_{max,h}^-$	Maximum electric power draw of the ground source cooling system
$P_{max,v}^\pm$	Vehicle on-board charger maximum power
$P_{app,h,t}$	Electric power draw of the appliances and lighting in house $h$ on hour $t$
$P_{sol,t}$	Photovoltaic power generation on hour $t$
$p_{r/m/F,t}$	Retail ( $r$ ) and market ( $m$ ) prices of electricity, as well as fuel ( $F$ ) prices on hour $t$
$p_f$	Additional fees included in retail electricity price
$Q_{cell/battery}$	Ampere-hour capacity of a single battery <i>cell</i> or a full <i>battery</i> system
$R_g$	Universal gas constant
$r_j$	Random number associated with type $j$ journey
$r$	PEV battery ageing model driving mode parameter
$SOC_0$	Battery ageing model fitting parameter
$SOC_{min}$	Minimum permitted SOC of the PEV batteries
$\bar{T}_{n,h,t}$	Mean temperature of node $n$ over all houses $h$ and hours $t$
$T_{n,v/h,t}$	Temperature of node $n$ for vehicle $v$ or house $h$ on hour $t$
$T_{sup,t}$	Heating system supply water temperature on hour $t$

$T_{max/min,n}$	Maximum or minimum temperature of node $n$
$T_{cell}$	Surface temperature of a single battery cell
$T_{dhw}$	Required domestic hot water temperature
$T_{in}$	Inlet cold water temperature
$T_g$	Yearly average temperature of the ground heat source
$T_s$	Surface temperature of the floor
$T_{op1.1}$	Operative temperature in the room at 1.1 m height
$U_p$	U-value of structural part $p$
$U$	Nominal voltage of the battery system
$V_{dhw,t}$	Volume of used domestic hot water per person on hour $t$
$w_{v,t}$	Vehicle $v$ grid-connection at work binary on hour $t$
$w_j$	Weight coefficient of type $j$ journey
$\mathbf{x}$	Vehicle node temperature vector
$\mathbf{y}$	House node temperature vector
$\mathbf{z}$	Vector containing the decision variables of a LP problem
$z_f$	Thickness of the modelled floor slab
$z$	Battery ageing model fitting parameter
$\alpha_n^{+/-}$	Vehicle heating (+) or cooling (-) element coefficient of performance of node $n$
$\alpha_{h,t}^{+/-}$	Coefficient of performance of the heating (+) or cooling (-) equipment of house $h$ on hour $t$
$\alpha_{ac}^-$	Seasonal energy efficiency ratio of the ground source cooling system
$\alpha_{hp,t}^+$	Coefficient of performance of the ground source heat pump on hour $t$
$\alpha_{dhw}^+$	Coefficient of performance of the heat pump for heating domestic hot water
$\alpha_c$	Battery ageing model fitting parameter
$\beta$	Vehicle thermal coefficient matrix 1
$\beta_{ij}$	Element of matrix $\beta$ on row $i$ and column $j$
$\beta_c$	Battery ageing model fitting parameter
$\gamma$	Vehicle thermal coefficient matrix 2
$\gamma_{ij}$	Element of matrix $\gamma$ on row $i$ and column $j$
$\gamma_c$	Battery ageing model fitting parameter
$\Delta t$	Time step length
$\Delta U_{tb}$	Extra heat transfer due to thermal bridging
$\delta T$	Temperature difference of the heat pump heat exchangers

$\epsilon_h$	House $h$ thermal coefficient matrix 1
$\epsilon_{h,ij}$	Element of matrix $\epsilon_h$ on row $i$ and column $j$
$\zeta_h$	House $h$ thermal coefficient matrix 2
$\zeta_{h,ij}$	Element of matrix $\zeta_h$ on row $i$ and column $j$
$\eta_{Ca}$	Carnot efficiency parameter
$\eta_k$	Energy efficiency of vehicle component $k$
$\kappa_{rfh/rad}$	Supply water temperature coefficient of floor heating ( $rfh$ ) or radiator heating ( $rad$ ) systems
$\Lambda_c$	Effective surface area of the vehicle cabin
$\mu$	<i>TABULA</i> reference air exchange rate
$\nu$	Hourly self-discharge rate of the battery system
$\bar{v}$	Mean total heat transfer factor between floor $f$ and interior $i$ nodes
$\tau_{rfh/rad}$	Supply water temperature constant of floor heating ( $rfh$ ) or radiator heating ( $rad$ ) systems
$v$	Total heat transfer factor between floor $f$ and interior $i$ nodes
$\Phi_{n,v/h,t}^{\pm}$	Total thermal power to node $n$ of vehicle $v$ or house $h$ on hour $t$
$\phi_{dhw,t}$	Thermal power required for domestic hot water per person on hour $t$
$\varphi_{ppl,h,t}$	Passive heating power of the residents of house $h$
$\varphi_{sol,h,t}$	Passive solar heat gains of house $h$ on hour $t$
$\Psi_{v,t}^{\pm}$	Total electric power of the battery management system and vehicle $v$ air-conditioning thermal elements on hour $t$
$\psi_{max,n,v}^{+/-}$	Maximum electric power draw of heating (+) or cooling (-) element of node $n$ of vehicle $v$
$\psi_{n,v,t}^{+/-}$	Electric power draw of heating (+) or cooling (-) element of node $n$ of vehicle $v$ on hour $t$
$\psi_{dhw,h,t}$	Domestic hot water heating electric power draw of house $h$ on hour $t$



## Abbreviations

A/C	Air conditioning
BEV	Battery electric vehicle
BMS	Battery management system
CD	Charge-depleting
COP	Coefficient of performance
CS	Charge-sustaining
DHW	Domestic hot water
DOD	Depth of discharge
DSM	Demand side management
HVAC	Heating, ventilation, and air conditioning
ICE	Internal combustion engine
LMO	Lithium-manganese oxide
LP	Linear programming
MG	Microgrid
MILP	Mixed-integer linear programming
MPC	Model predictive control
NMC	Nickel manganese cobalt
PDF	Probability density function
PEV	Plug-in electric vehicle
PHEV	Plug-in hybrid electric vehicle
pp	Percentage point
PV	Photovoltaic
RE	Renewable energy
<i>SEA</i>	<i>Swedish Energy Agency</i>
SHLC	Space heating load control
<i>SMHI</i>	<i>Swedish Meteorological and Hydrological Institute</i>
<i>SIKA</i>	<i>Swedish Institute for Transport and Communications Analysis</i>
SOC	State of charge
UDDS	Urban dynamometer driving schedule
V2G	Vehicle-to-grid



# 1. Introduction

The amount of renewable energy (RE) generation in the world is steadily increasing along with energy demand [1]. Concerns about the adverse effects of fossil fuel and nuclear based generation are driving the change towards a more sustainable energy economy, one where decentralized RE generation would hold a more central role. However, some prominent RE technologies, such as solar and wind generation, are rather unpredictable by nature and often don't coincide with energy demand.

Any electrical grid must balance generation and consumption at all times in order to function properly. Traditionally power systems have been designed as load-following, with the generation side adjusting its output to meet the demand in order to ensure grid stability. However, this type of grid stabilization is becoming increasingly more difficult with the growing penetration of variable RE generation. Without additional flexibility offered by other generators, consumers, or energy storage facilities, large scale RE generation cannot be fully utilized without compromising grid reliability and safety. [2]

In principle, energy storage has the potential to solve the RE mismatch problem, as well as reduce the need for expensive peak-load power plants operated only out of necessity at high marginal cost. Unfortunately, electricity is a difficult form of energy to store economically. Storage technologies with good electricity conversion efficiencies are typically set back by large self-discharge rates, making them infeasible for long-term seasonal storage, and their high cost usually makes them less attractive a storage option than comparable thermal storages. [3]

Demand side management (DSM) is a concept that aims to compensate the generation side loss of flexibility by establishing some manner of control over the consumption. In principle, DSM encompasses all activities by the consumer side that affect the electricity demand, from changing appli-

ances to more efficient ones to rescheduling appliances or even curtailing some consumption altogether. In current power systems, DSM consists mostly of large industrial consumers having agreements with the grid operators to reduce their consumption during peak hours, should the need for it arise. [3]

With the expansion of time-of-use and real-time pricing, DSM is slowly starting to spread to customer driven applications as well. In addition, the rapid developments in communication technologies and increasing networking of appliances have enabled controlling individual appliances in accordance with the needs of the consumer and the electrical grid. This form of DSM is often referred to as *load shifting*, and can naturally only be applied to a small subset of appliances, as consumers cannot be expected to schedule their entire lives around RE generation. Ideally DSM appliances have a lot of idle time, and the exact timing of their power draw is irrelevant to the end user. For example space heating, heating domestic hot water (DHW), and charging plug-in electric vehicles (PEVs) are promising candidates for DSM applications. [3]

As the transportation sector is heavily dependent on oil, transport electrification is seen as an appealing approach to reducing greenhouse gas emissions, and the market penetration of PEVs is expected to increase significantly in the years to come. PEVs can be further divided into two distinctively different categories: battery electric vehicles (BEVs) that are fully electric, and plug-in hybrid electric vehicles (PHEVs) that also have an on-board internal combustion engine (ICE) for propulsion and or electricity generation. Since most privately owned vehicles spend significant amounts of time parked [4], with PEVs this means a considerable amount of idle battery capacity connected to the grid. Using smart charging a fleet of PEVs could provide a significant contribution to the flexibility of the electrical grid. The vehicle-to-grid (V2G) concept aims to take the interaction between PEVs and the electrical grid a step further, by making it possible for the PEVs to feed electricity back into the grid. Essentially, this would render the PEV fleet a form of mobile distributed short-term electricity storage. [5]

Even with sufficient flexibility, operating country-wide electrical grids safely and reliably is a difficult task, which is made no easier by the increasing amounts of distributed generation. Microgrids (MGs) are a conceptual solution that aims to divide the overlaying power grid into smaller self-regulated sub-grids, making it easier to manage the grid as a whole.

Essentially, MGs are comprised of various loads and distributed generators operating under some sort of an energy management system ensuring that the MG behaves according to the needs of the overlaying electrical grid. The most significant feature of MGs is the possibility to make them capable of autonomous operation while disconnected from the main grid, often referred to as *islanded operation* in literature. [6]

This work aims to determine what the benefits achievable by V2G and space heating load control (SHLC) schemes are for residential-scale consumers with local photovoltaic (PV) generation. What are the savings in yearly electricity costs for different PEV and SHLC systems, and how are they affected by the number of households in the MG, the amount of PV generation, or PEV battery degradation? These questions are addressed by constructing a linear programming (LP) model of a small residential MG with PEVs and PV generation, and cost-optimizing the scheduling of the PEV and space heating loads.

The thesis is organized as follows: Chapter 2 provides a review of the state-of-the-art literature on the various technological concepts modelled in this work, Chapter 3 explains the various derived models and sources of data, and Chapter 4 explains the final LP formulation. Chapter 5 presents and discusses the results, and finally Chapter 6 presents a summary and conclusions of the work.

## 2. Background

In this work V2G and SHLC are studied as energy management assets for residential customers in increasing the self-consumption of locally produced PV, as well as for taking advantage of real-time pricing. The MG concept offers us a great platform to aggregate the benefits of PV generation combined with the storage capacity provided by the PEVs and thermal mass of the modelled houses, although such a system would naturally require the co-operation of the inhabitants.

The followings sections further describe the various aforementioned concepts, as well as provide a quick overview on the relevant literature. State-of-art studies relevant to the aims of this work are also described in more detail.

### 2.1 Space Heating Load Control

Space heating load is an ideal candidate for DSM, as the exact timing of the power draw is of no consequence to the consumer as long as thermal comfort isn't compromised. Depending on the heating system, the thermal mass of the building, as well as possible thermal energy storage elements such as hot water storage tanks or phase change materials, the space heating load can incorporate considerable amounts of flexibility. Naturally, taking advantage of the buildings properties in this manner requires sophisticated control schemes for the heating system, for example model predictive control (MPC). MPC is a method that aims to utilize the thermal storage in a building to its maximum potential via model-based predictions of the building's climate, that attempt to account for disturbances such as internal heat gains and weather. [7]

Applications for heating, ventilation, and air conditioning (HVAC) load control have been widely studied in literature, ranging from grid ancillary

services with both commercial [8] and residential buildings [9], to economical energy management again with both commercial [10] and residential [11] scale buildings. As grid ancillary services and commercial buildings are beyond the scope of this work, the rest of the literature review shall focus on residential scale energy management studies.

MPC is considered well suited for SHLC, for example a study by *R. Havlgaard et al.* [12] presents a MPC scheme that is designed to minimize the heating costs of a modelled residential house with a ground source heat pump and a floor heating system. The simulation spanned a 5 day period with the controller having access to perfect forecasts on weather and electricity prices for the next 2 days, and the MPC was able to achieve 25% cost savings over a constant electricity price scenario without compromising thermal comfort.

In another study by *B. Favre and B. Peuportier* [13], dynamic programming was used for SHLC in a low energy single-family house in France with time-of-use pricing and no active thermal storage elements. The cost optimal scheduling of the space heating load resulted in 10–30% reduction in heating costs over a constant temperature control scheme during the modelled week during winter depending on the modelled weather, even though utilizing the thermal mass of the house was found to lead into increased heating energy consumption of 3–15%. The study also highlights the importance of building thermal mass and insulation for the flexibility of the space heating load.

*M. Ali et al.* [14] on the other hand used LP optimization in their study of a Finnish single-family house with direct electric heating and partial thermal storage, using hourly spot market electricity prices. The optimizations were performed during a winter day with unusually volatile spot market prices, and resulted in heating cost savings from around 5.5% for no thermal storage up to around 46% with thermal storage capacity capable of storing 40% of daily heating demand, when compared to an unoptimized scenario.

While the aforementioned studies have focused mainly on reducing heating costs under various time-of-use electricity prices, *D. Vanhoudt et al.* [15] performed a laboratory test of a residential heat pump emulating the behaviour of a residential single-family house, with sufficient PV or wind generation to render the modelled house a net-zero energy building. The emulated house had a floor heating system and included a 400 l hot water storage tank for thermal storage, as well as a 300 l DHW

tank. The used market-based multi-agent control system increased RE self-consumption by 5–29% in all studied RE scenarios when compared to conventional heat demand based controls during the simulated winter weeks. However, the multi-agent controls also increased the overall energy consumption of the heating system by around 8-12%, making the reduction in electricity bought from the main grid insignificantly small.

While the aforementioned studies have modelled and optimized the SHLC of single-family houses in great detail, most of the studies seem to span only a few weeks at best. In addition to examining the yearly benefits of SHLC in this work, we also study the effects of increasing the number of co-operating houses in the modelled MG combined with PEVs. To the author’s best knowledge, the effects of this type of scaling haven’t been previously studied in literature.

## 2.2 PEV Smart Charging and Vehicle-to-Grid

Since PEVs represent a significant extra load for the electrical grid, smart charging is expected to become a crucial part of vehicle electrification in order to avoid adverse effects of uncoordinated charging [16, 17]. In addition to avoiding overloading the power grid, smart charging has been shown capable of providing benefits such as cost savings [18], peak load reduction [19], and increased battery lifetime [20].

The V2G concept aims to take smart charging a step further by enabling the PEVs to feed electricity from their batteries back into the grid, effectively rendering the PEV fleet a massive mobile distributed electricity storage, and some even envision that PHEVs could generate electricity for the grid using their ICEs [5]. However, successfully implementing V2G technology in the existing power systems is challenging. The requirements on the charging infrastructure include fast and safe power connection with the grid, communications between the PEV and the grid operator, and suitable metering. Incorrect usage of the V2G systems could result in adverse effects on the distribution equipment in the grid, as well as unnecessary battery degradation. Even system security has to be considered to eliminate the possibility of deliberate misuse. [21]

As a concept, V2G was first proposed by *W. Kempton and S. Letendre* [22], where they highlight the potential of the technology as a buffer for RE generation or as a peak power resource and provide a simple economic evaluation of the possible benefits. The larger scale studies on the vari-



ous applications of V2G include wind [23] and PV [24] integration on a national scale, as well as grid ancillary services using thousands of PEVs [25]. V2G has also been studied as a way to increase MG reliability, particularly under islanded operation [26]. As this work focuses on RE integration and energy management, a few of such studies will be discussed in more detail below.

*C. Battistelli et al.* [27] proposed an optimization tool, in which a LP algorithm is used for energy management in a large MG. The case study consists of two V2G-capable garages, a biomass power plant, a wind farm, and appropriate loads derived from typical residential and industrial profiles. Robust optimization was used to account for the uncertainty associated with the number of PEVs connected into the grid, and uncertainty in the wind power production was accounted for by a stochastic programming framework. According to the study, PEV availability is the main source of uncertainty in this type of energy management optimization.

RE integration via V2G has been studied by *M. Honarmand et al.* [28] in a MG with micro-turbines and fuel cells for additional distributed generation using mixed-integer linear programming (MILP) methodology. The PEVs were connected to the MG via an intelligent parking lot acting as an aggregator for the distributed PEV batteries, and possible consequences of battery degradation were acknowledged by reducing the permitted cycling of older PEV batteries. The proposed energy resources scheduling results in lower overall operating costs in the modelled MG, as well as points out the intelligent parking lot could provide cheaper spinning reserves for the MG than the fuel cells and micro-turbines. RE integration and energy management of PEVs in a MG has also been studied by *W. Su et al.* [29], using two-stage stochastic optimization in order to account for the inherent uncertainty of RE generation.

Optimal energy management in a single household with V2G and RE generation has been studied by *L. Igualada et al.* [30]. The presented MILP model divides the household electricity load into *critical*, *adjustable*, and *shiftable* categories, and includes simple battery wear cost calculations. A novel representation of range anxiety is also included, in the form of a parameter that penalizes the PEV battery for incomplete state of charge (SOC). The study reports overall daily electricity cost savings up to €0.52 (15.5%) for the simulated house depending on the simulated level of range anxiety, compared to the daily cost of electricity of €3.33 for the baseline case where the PHEV charges itself to full as soon as possible.

*M. Rastegar and M. Fotuhi-Firuzabad* [31] have also studied household V2G energy management, with both RE and natural gas fuelled CHP. Their modelled household also included a separate 7.8 kWh electricity storage as well as a dispatchable dishwasher, washing machine, and a clothes dryer. The study resulted in the yearly total costs decreasing from €1801 to €631 (65% reduction) when installing 20 m<sup>2</sup> of PV (around 5 kW<sub>p</sub>) and enabling V2G in their modelled household.

The aforementioned studies have experimented with a multitude of different scenarios, optimization methods, and objectives for V2G technology. However to the author's best knowledge, the effects of V2G on PEV battery lifetime are often omitted, or acknowledged through approximations based on the number of battery cycles, neglecting the impact of battery temperature and exact PEV utilization on the cycle life.

### **2.3 Battery Management Systems and Battery Ageing**

The battery systems in PEVs consist of hundreds of small battery cells, which are assembled into battery modules, which are then connected into the full battery system and regulated by a battery management system (BMS). The main tasks of the BMS are ensuring that the individual battery cells operate within proper voltage and temperature intervals while fulfilling the requirements of the PEV. The voltage interval requirements are met with various systems to detect, estimate, and equalize parameters such as current throughput and SOC. As such systems are electronic, their energy consumption is likely insignificant for the PEVs. However, ensuring the correct operating temperature of the battery system is usually done with air or liquid thermal management systems [32]. Especially in colder climates, heating the battery during winter could prove to affect the PEV usability. [33]

So far the applications of batteries haven't required extensive lifetimes, but for automotive applications understanding the ageing phenomena and their implications on the performance of batteries has become crucial. Identifying different ageing and degradation mechanisms that occur in batteries is a difficult task, as the processes are often complicated and depend on both environmental and utilization related parameters. The battery ageing process can be divided into two distinctive parts, called *calendar ageing* and *cycle ageing*. Calendar ageing is the degradation of battery performance associated with self-discharge and storage, whereas

cycle ageing is the degradation associated with the charging and discharging processes. [34]

Currently the PEV industry seems to prefer various Li-ion chemistries due to their high specific energy, comparatively low cost, as well as sufficient performance and lifetime [35]. The ideal battery temperature for Li-ion batteries is between 25°C to 40°C when in use, where a good balance between battery performance and degradation is reached [32]. However, thermal management systems consume on-board energy from the vehicle battery when the PEV isn't plugged in, reducing the range of the vehicle. In reality PEV manufacturers seem to prefer the extended range over the reduced battery degradation. The thermal management systems in real PEVs seem to be set to keep the battery temperature within safe discharging limits between around -30°C to 55°C, depending on the exact battery chemistry [33]. For example, the *Nissan Leaf 2013 Owner's Manual* [36] states that the battery warmer turns on if the Li-ion battery temperature is -17°C or lower, whereas the *Mitsubishi I-MiEV 2012 Owner's Manual* [37] states that the battery is heated only when its temperature is below -25°C. Charging the batteries however is another matter, as below 0°C lithium plating of the anode may occur, significantly reducing the cycle-life of the battery [38].

Battery ageing in PEVs has been thoroughly studied by *K. Smith et al.* [39] and *J. Neubauer et al.* [40], under varying battery temperatures and drive cycles necessary to correctly account for PEV use. While these studies haven't included V2G, they provide valuable information on the role of battery and cabin thermal management in the PEV energy consumption and battery ageing. According to [40], the primary challenges for PEVs in cold climates are efficient cabin heating systems, while the impact of required battery heating remains largely negligible. In hot climates on the other hand, efficient battery cooling systems were considered necessary to avoid excessive battery degradation.

The feasibility of V2G as a peak power resource considering battery ageing has been studied by *C. Zhou et al.* [41], taking into account the depth of discharge (DOD) of the batteries and the ambient temperature. However, the modelling is simplified by removing any thermal management elements from the batteries. The study concludes that only Li-ion batteries might be economical under temperate climate conditions for V2G, whereas lead-acid and nickel-metal hydride chemistries aren't due to lower cycle life.

A simple battery degradation model for PEV modelling was also proposed by *S. Han et al.* [42], and demonstrated with optimizing residential V2G energy management with PV generation. The battery wear model is extremely simplified in order to allow for calibrating the model to correspond to different battery chemistries according to typical cycle-life data provided by battery manufacturers, and neglects the effects of battery temperature. However, the study shows that including the approximated costs of the battery wear in the energy management optimization has a considerable impact on the V2G behaviour of the PEV. The PEV was seen limiting its V2G use to times when the benefits exceeded the costs, but ultimately the results could not be considered economical with the modelled battery costs.

### 3. Data and Modelling

The *Swedish Energy Agency (SEA)* carried out a monitoring campaign covering 201 detached houses and 188 apartments between August 2005 and December 2008 [43], most of which were located in the Mälardalen region (58–59°N, 15–18°E). All the major electric equipment in the measured houses were monitored with wattmeters, from the HVAC system down to the individual appliances and lights. The electrical energy consumptions of each monitored device were logged with a 10-minute time resolution. Even though the study was conducted several years ago, it is reasonable to assume that there have been no significant changes in residential electricity consumption since then, with the possible exception of lighting [44].

From this data, 5 detached houses and 5 apartments that were measured for a full year during the years 2005–2006 were selected to represent the households modelled in this work. The data of the selected households was rearranged to form uninterrupted electricity consumption profiles spanning from 2005-9-1 00:00 to 2006-8-31 23:00 for each household, essentially assuming that the electricity consumption habits were unaffected by weather or electricity prices. As the space heating load of the houses is modelled separately for DSM purposes, this is a reasonable assumption.

In this work, we build a residential energy management optimization model, which is illustrated in Figure 3.1, based on the aforementioned data. The following sections explain the various models used to describe a single-family household with a PEV and local PV generation, as well as any additional data used in their construction. Hourly time scale is used mainly due to lack of more accurate weather and driving pattern data, but also to allow for faster computations spanning the entire modelled year.

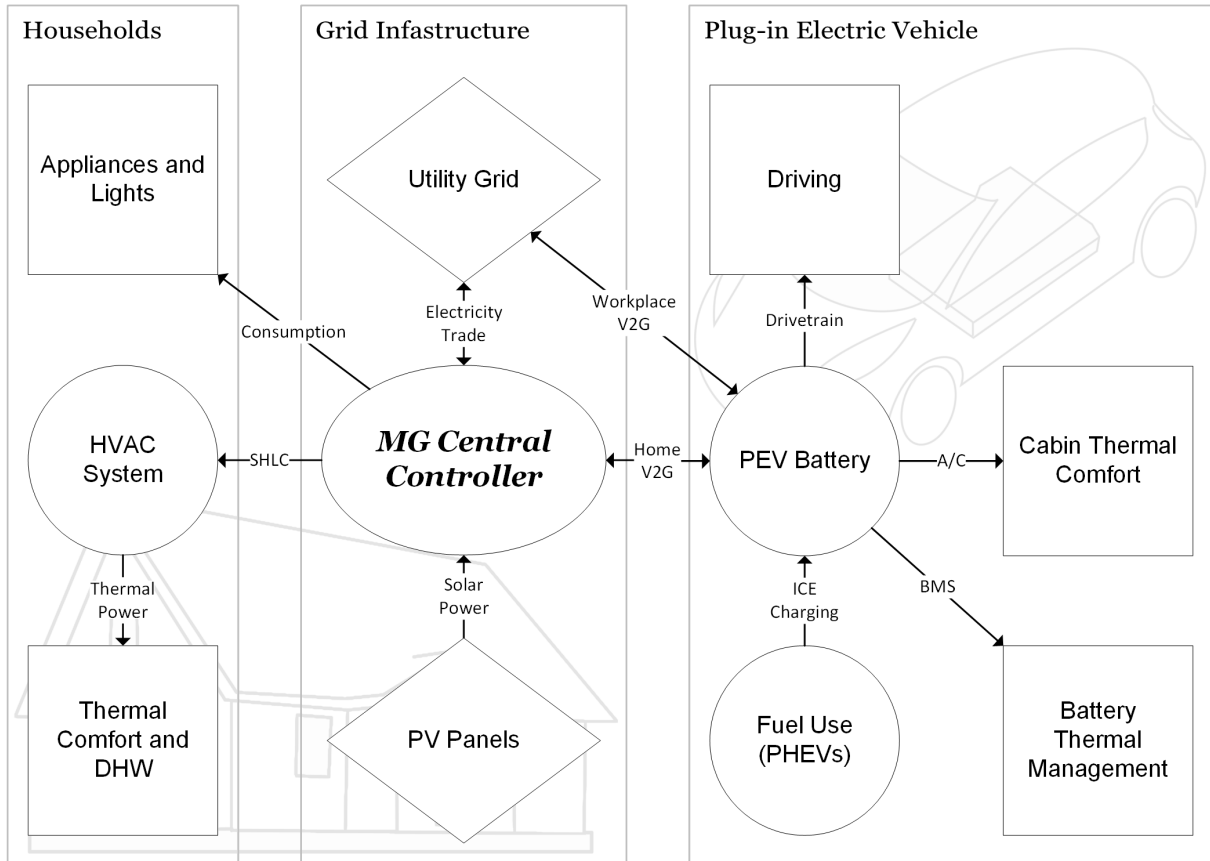


**Figure 3.1.** Illustration of the energy flows within the modelled residential MG. The energy management is centrally optimized, meaning that each HVAC system and PEV is co-operating towards a single common goal. The circles represent dispatchable devices, the diamonds represent electricity infrastructure, and the squares represent required uses for energy.

### 3.1 PEV Availability and Movement

The biggest difference between a PEV and a regular electricity storage is that the PEV is also used for travelling, and thus is not always available as a dispatchable resource. Also unlike stationary electricity storage systems, the PEVs have more strict temporal constraints on their SOC, as they need to be sufficiently charged in order to complete necessary trips at specific times.

A national travel survey by the name of *RES 2005–2006* [4] was conducted in Sweden between October 2005 and September 2006 by *Statistics Sweden* and *Swedish Institute for Transport and Communications Analysis (SIKA)*. The survey included telephone interviews supported by travel journal entries, and consists of data obtained from slightly over 41,000 randomly selected people between the ages of 6 and 84. Each participant recorded their movements on a single specific day of survey, determined by the *SIKA*. The raw travel journal data was not available, and instead we

use the public statistics, which allow us to generate approximate driving patterns for typical Swedes, albeit some assumptions have to be made.

The hourly distribution of journeys by purpose as determined in the *RES 2005–2006* survey statistics is shown in Figure 3.2. Unfortunately, the statistics don't differentiate between going to and returning from work, combining them into a single category instead. The *RES 2005–2006* questionnaire definition of a *journey* is a set of consecutive trips with either residence, workplace, or school as possible final destinations [4]. This results in *trips* from home to work and from work back home counting as separate *journeys*, whereas *trips* from home to a shop and back again count as a single *journey*. The survey also divided each *trip* into *stages* if the mode of travel changed mid-travel, for example driving to a train station and travelling the rest of the way via train.

Assuming that each person has to both go to work and return from work during a single day and that the number of people going to work and returning from work are equal, the work journey distribution can be cut in half to form two separate distributions for these different trips. Since the different distributions have their minima at 01:00–01:59 as seen in Figure 3.2, we'll choose to have it represent the point at which every person returns from work or other journeys at the latest. Then by choosing 11:00–

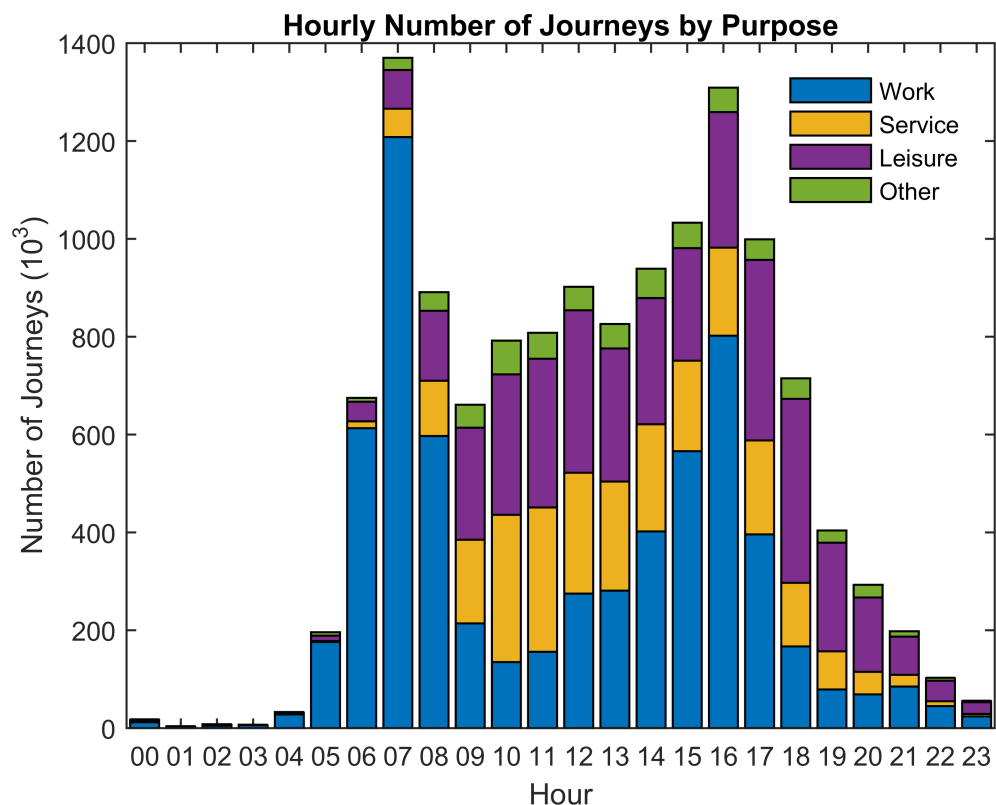


**Figure 3.2.** The hourly distribution of journeys by purpose [4].

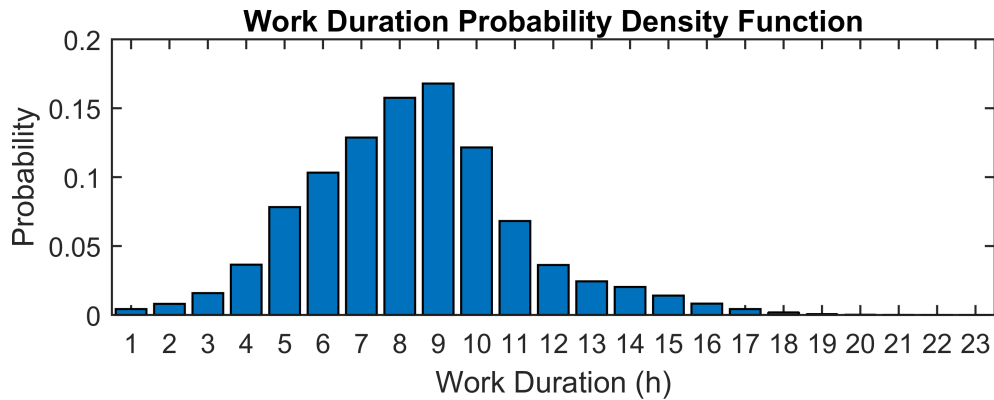


**Figure 3.3.** The PDF of work duration including commuting. Calculated from PDFs for going to work  $f_g$  and returning from work  $f_r$  that are assumed to be independent of each other.

11:59 as the latest hour people go to work, we minimize the difference between the number of trips to and from the workplace. This yields two separate hourly distributions that can easily be normalized into discrete probability density functions (PDFs). In reality, the PDFs of going to work  $f_g(t_g)$  and returning from work  $f_r(t_r)$  aren't independent, but instead are linked together by a work duration distribution  $f_w(\Delta t_w)$ , which unfortunately is unknown. For now, we assume  $f_g$  and  $f_r$  to be independent and calculate the work duration PDF as

$$f_w(\Delta t_w) \simeq \sum_{t_g} f_g(t_g) f_r(t_g + \Delta t_w). \quad (3.1)$$

The resulting PDF presented in Figure 3.3 has a reasonable shape, even though it includes possible work durations up to 19 hours. However, this work duration distribution essentially gives the amount of time the PEV spends parked at the workplace, and not the amount of time the commuters are expected to actually work. Thus the occasional longer work days can be interpreted as occurrences where the commuters spend time in the vicinity of the workplace while leaving their PEV parked there. Similarly, the occurrences where the work duration is exceptionally short could be interpreted as occasions where the commuters only shortly visit their workplace, and work from home for the rest of the day.

From here on, we define *journey* as the whole act of travelling away from *home* in order to perform a task and returning later, whereas *trips* are defined as the individual acts of moving between places. As an example, a normal workday counts as a single *work-type journey* under this definition, and includes two *trips*: going to and returning from work.

As for the journeys unrelated to working, certain assumptions also have to be made in order to extract applicable PDFs from the statistics. First,



we assume that each PEV can only make one journey for each purpose on each day, but besides commuting on workdays isn't required to make any. Second, the *service*, *leisure*, and *other*-type journey PDFs  $f_s(t)$ ,  $f_l(t)$ , and  $f_o(t)$  can be normalized so that

$$\sum_{t=1}^{24} w_s f_s(t) + w_l f_l(t) + w_o f_o(t) = \frac{N_Y}{N_Y + N_N}, \quad (3.2)$$

Where  $w_s$ ,  $w_l$ , and  $w_o$  are weight coefficients determined by the relative numbers of the different journey types,  $N_Y$  is the number of people that travelled on their day of survey, and  $N_N$  is the number of people that didn't. Third, the weight coefficients are determined by the relative numbers of journeys made by car for each purpose. The resulting PDFs for the different types of journeys are presented in Figure 3.4.

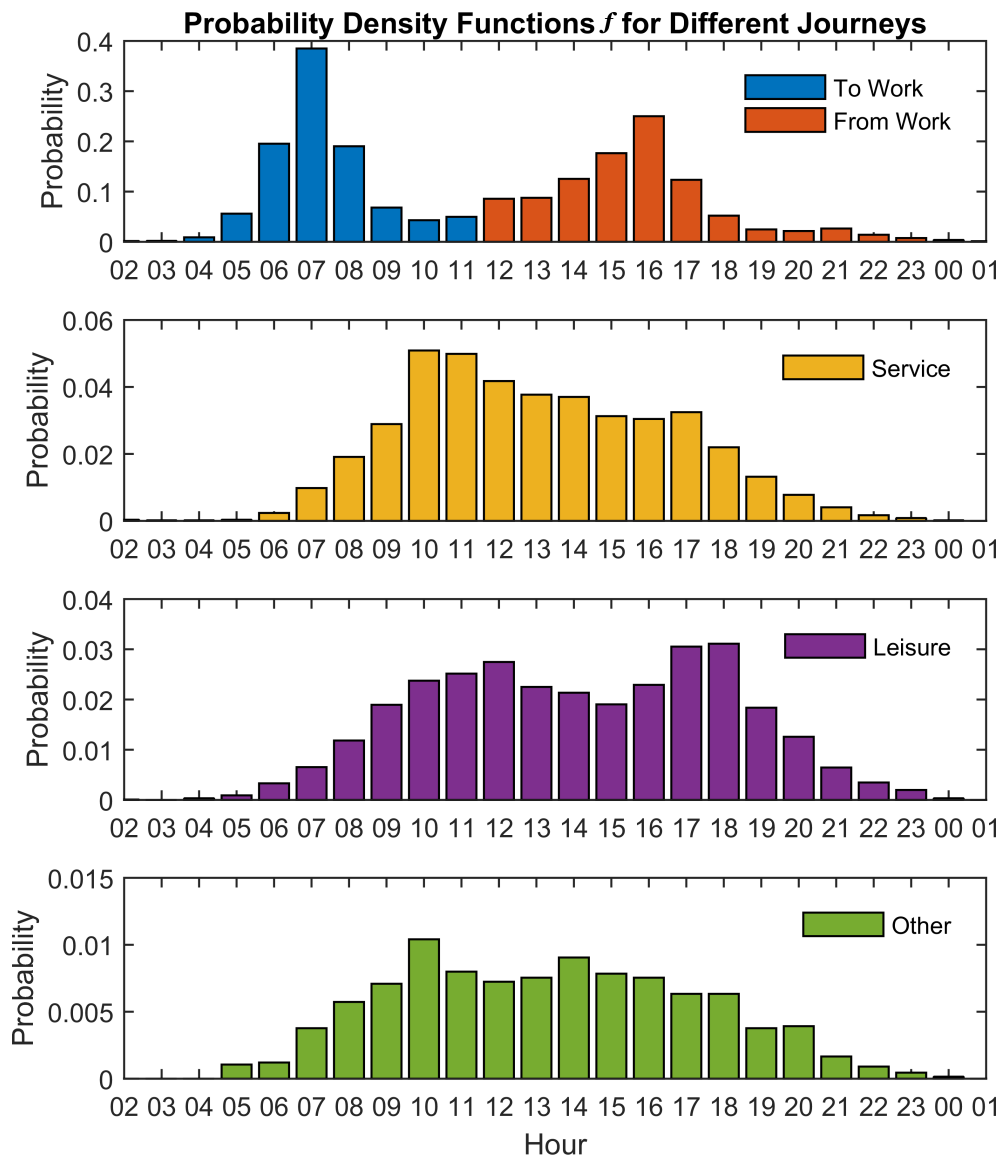


**Figure 3.4.** The PDFs for different trips used in generating the driving patterns of each vehicle.

Each type of trip has a set distance driven, determined by the average *stage* lengths of the *car driver* category in the *RES 2005–2006* [4] statistics, which are used in calculating the driving electricity consumption time series for each PEV. The lengths of the trips are considered to be independent of the PEV's location for simplicity, implying that a trip to the shop is equally long whether the car is at home, at work, or on another journey. If multiple trips are made on the same time step, only the longest trip will count in order to prevent excessive driving during a single hour. This can be interpreted as combining multiple tasks into a single trip, for example stopping to buy groceries on the way home from work.

The movement time series of each PEV are generated in 24-hour segments starting at 02:00 each day, which was previously chosen to represent the latest hour every PEV returns home at the latest, using the journey PDFs and the following procedure:

1. PEV location initialized to *home*  $\forall t \in [1, 24]$ .
2. Generate independent uniformly distributed random  $\{r_g, r_w, r_s, r_l, r_o\} \in [0, 1]$ .
3. **If** it is a workday.
  - **Find**  $\min(t_g)$  *s.t.*  $\sum_{t=1}^{t_g} f_g(t) \geq r_g$ ,  $t_g \in [1, 24]$ .
  - **Find**  $\min(\Delta t_w)$  *s.t.*  $\sum_{\Delta t=1}^{\Delta t_w} f_w(\Delta t) \geq r_w$ ,  $\Delta t_w \in [1, 24]$ .
  - PEV location set to *work* on hours  $t_g$  to  $t_g + \Delta t_w$ .

**Else** no *work* journey is made today.
4. **Find**  $\min(t_s)$  *s.t.*  $\sum_{t=1}^{t_s} f_s(t) \geq r_s$ ,  $t_s \in [1, 24]$ .  
**If**  $\sum_{t=1}^{24} f_s(t) < r_s$ , no *service* journey is made today.  
**Else** set PEV location to *service* on hour  $t_s$ .
5. Repeat step 4 for *leisure* and *other*-type journeys.
6. Update the PEV location time series.
7. Repeat steps 1-6 for the next 24 hours.

The *service*, *leisure* and *other* type journeys are determined in exactly this order because then possible overlaps result in the longer journeys over-

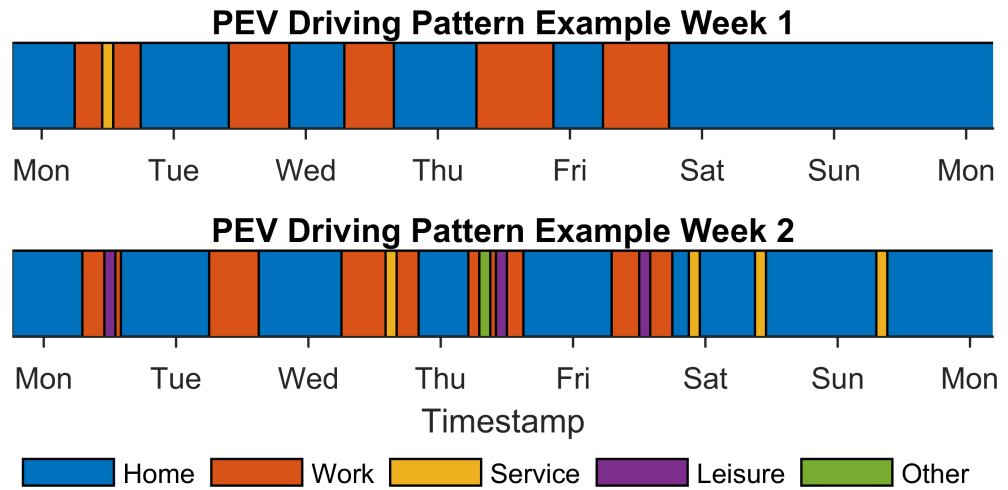


**Figure 3.5.** Examples of the possible of the driving patterns generated. *Week 1* barely has any trips besides commuting, whereas *Week 2* has non-commuting trips almost every day.

writing the previous one. The random numbers are generated using the *Mersenne Twister*, and unless otherwise mentioned all the simulations presented in this work use the same generation seed (0) resulting in the same driving profiles. Figure 3.5 presents two example weeks of generated driving patterns, that represent different extreme cases.

It is worthy of note that the way the PDFs are derived from the statistics permit *service*, *leisure* and *other* journeys during workdays at the same probability than during weekends, which can result in some heavy driving during working hours as can be seen from Figure 3.5. For BEVs this can cause problems if the vehicle is required to drive extensive distances without a chance to recharge the battery.

The energy consumption of cars is dependent on the ambient temperature, mostly because of air conditioning (A/C). For traditional ICE vehicles and PHEVs, the waste heat from the engine is often used to assist in cabin heating, reducing the impact of cold ambient temperatures on the driving energy consumption [45, 46]. For BEVs however, the A/C system has to draw comparatively more power from the battery in order to manage the cabin temperature, reducing the range of the vehicle when A/C is employed. In hot ambient conditions, such as Phoenix, Arizona, the energy demands of PHEVs and BEVs are much more similar [40].

The energy consumption of the PEV drivetrain is assumed to be independent of the ambient temperature, and the increased energy consumption while driving in cold or hot ambient temperatures is only accounted for by the cabin A/C and BMS. The base driving energy consumption of the drivetrain is calculated by multiplying the driving distance with the av-

average energy consumption per kilometre of the vehicle, measured at 23°C with vehicle A/C systems off for the urban dynamometer driving schedule (UDDS) [47, 48], which simulates driving in an urban environment.

Experimental data related to the energy consumptions of various PEVs under different driving conditions were obtained from the *Downloadable Dynamometer Database* [48], and experimental data related to the technical specifications of various PEVs were obtained from the *Advanced Vehicle Testing Activity* [47] database. The values of the parameters related to the PEV modelling are presented in Tables 3.1 and 3.2.

### 3.2 PEV Batteries and Thermal Management

The performance of a battery system is mainly dependent on its temperature and SOC. In cold ambient temperatures, the increase in internal resistance generally makes fully charging or discharging the battery take longer, as the current must be lowered earlier in order to keep cell voltage within permissible limits [49]. For our purposes the decrease in the maximum discharging power can be neglected, as PEV battery systems are designed with a high peak power capability ( $\approx 50\text{--}120$  kW [47]) required for sufficient driving performance. Thus, the electric infrastructure between the PEV and the utility grid sets the limit to the V2G discharge.

The reduction in charging power in cold ambient temperatures is a more difficult matter. Measurements in different ambient temperatures indicate that the time required for a full charge for the *2013 Nissan Leaf* increases by around 15–40 minutes when the ambient temperature decreases, as can be seen from Figure 3.6 [47]. The total charge delivered into the battery remains approximately the same regardless of charging temperature, but this might vary depending on battery chemistry. Both modelled real-world vehicles, *Nissan Leaf* and *Chevrolet Volt*, have batteries with lithium-manganese oxide (LMO) cathodes and carbon anodes (LMO/Carbon). The effect of temperature on the battery system performance can thus be assumed to be approximately the same.

Properly accounting for the temperature dependency of the battery performance would require modelling the battery system down to its voltage and current characteristics, which would necessitate non-linear optimization methods for optimal control as well as shorter time steps, reducing computational efficiency. On an hourly time step, the temperature dependency of the battery power can be safely neglected.

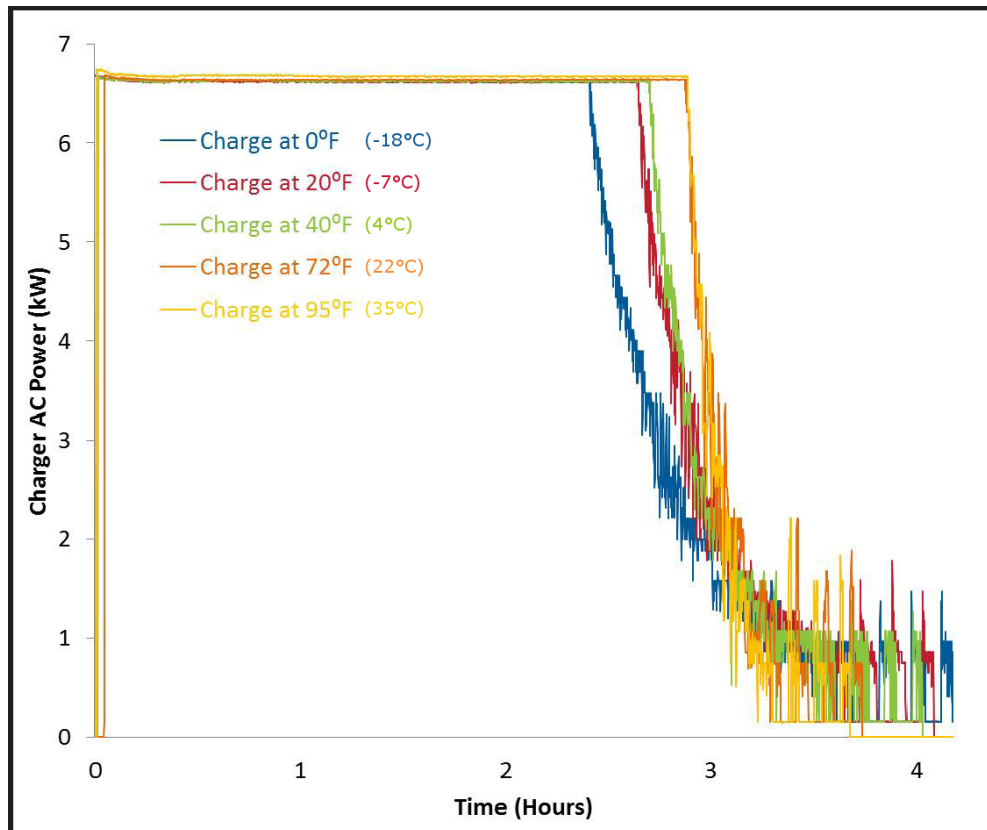


**Figure 3.6.** Nissan Leaf charging power consumption in different ambient temperatures. At cold ambient temperatures the power has to be reduced earlier, but the energy after the full charge is roughly the same at all temperatures. Reproduced from [47] with added °C temperature readings.

### Battery Energy Model

For our purposes, the dynamics of a V2G-ready PEV battery module can be written as

$$\frac{dE(t)}{dt} = \eta_b \eta_c (P^+ + \eta_F F^+) - P^- - D^- - \Psi^\pm - \nu E(t), \quad (3.3)$$

where  $E(t)$  is the energy stored in the battery module of the car,  $\eta_b$  is the battery charging and discharging efficiency,  $\eta_c$  is the efficiency of the on-board battery charger,  $P^+$  and  $P^-$  are the grid connected charging and discharging power terms respectively,  $\eta_F$  is the fuel-to-electricity efficiency of the ICE and  $F^+$  is the fuel energy consumption term,  $D^-$  is the power draw required by driving the PEV,  $\Psi^\pm$  is the total electric power of the BMS and vehicle A/C thermal elements, and  $\nu$  is the self-discharge rate of the battery system. The self-discharge rates of Li-ion batteries typically range from 3–5% per month [33], resulting in hourly self-discharge rates around  $\nu < 10^{-4} \frac{1}{h}$ . This value is insignificantly small when considering how PEVs are used, but without any storage losses the battery model can run into numerical issues where the optimized control charges the battery in pulses every other hour, presumably to take advantage of

limited numerical accuracy and rounding. Strictly speaking the battery efficiency  $\eta_b$  alone would be enough to counter this problem, but the self-discharge can be included explicitly without adding to the complexity of the model. Values for the various parameters are presented in Table 3.2. Assuming that the different power terms stay constant over a time step  $\Delta t = 1$  h, Eq. (3.3) can be solved

$$\begin{aligned}
\frac{dE(t)}{dt} + \nu E(t) &= \eta_b \eta_c (P^+ + \eta_F F^+) - P^- - D^- - \Psi^\pm & \left| \cdot e^{\nu t} \right. \\
\frac{d}{dt} \left( E(t) e^{\nu t} \right) &= e^{\nu t} [\eta_b \eta_c (P^+ + \eta_F F^+) - P^- - D^- - \Psi^\pm] & \left| \int_t^{t+\Delta t} dt \right. \\
\left( E(t) e^{\nu t} \right) \Big|_t^{t+\Delta t} &= \left( \frac{e^{\nu t}}{\nu} \right) \Big|_t^{t+\Delta t} [\eta_b \eta_c (P^+ + \eta_F F^+) - \dots] & \left| \cdot e^{-\nu(t+\Delta t)} \right. \\
E(t+1) - e^{-\nu \Delta t} E(t) &= \frac{1 - e^{-\nu \Delta t}}{\nu} [\eta_b \eta_c (P^+ + \eta_F F^+) - \dots] & \left| \cdot \frac{\nu}{1 - e^{-\nu \Delta t}} \right.
\end{aligned}$$

and written using time step indexing

$$\frac{\nu}{1 - e^{-\nu \Delta t}} (E_{t+1} - e^{-\nu \Delta t} E_t) = \eta_b \eta_c (P_t^+ + \eta_F F_t^+) - P_t^- - D_t^- - \Psi_t^\pm, \quad (3.4)$$

where  $t$  is the time step.

For simplicity, the PHEV is assumed to always work in series operating mode, meaning that the on-board ICE is used solely for generating electricity to the battery system. In reality, the *Chevrolet Volt* PHEV modelled in this work is actually a so-called multi-mode hybrid. Thus it would be capable of also operating in power-split mode, meaning that the ICE could be used to provide power directly to the wheels bypassing the battery and the electric motor.

The assumption that the power terms for fuel usage  $F_t^+$ , driving  $D_t^-$ , and vehicle thermal elements  $\Psi_t^\pm$  remain constant over an entire hour is rather unrealistic, as most of the modelled trips only take around half an hour [4]. Fortunately the energy balance dynamics determined by Eq. (3.4) are insensitive to the length of the time step, since the battery energy depends more on the amount of energy drained than its exact timing.

### Vehicle Thermal Model

In this work the thermal behaviour of the PEVs is modelled using a two-capacity model for simplicity and computational efficiency, illustrated in Figure 3.7. The energy balance equations for the vehicle cabin and battery nodes can be written as

$$C_b \frac{dT_b(t)}{dt} = H_{be}(T_e - T_b(t)) + H_{bc}(T_c(t) - T_b(t)) + \Phi_b^\pm, \quad (3.5)$$

$$+(1 - \eta_b)(\eta_c P^+ + P^- + \eta_F \eta_c F^+ + D^-)$$

$$C_c \frac{dT_c(t)}{dt} = H_{ce}(T_e - T_c(t)) + H_{bc}(T_b(t) - T_c(t)) + \Phi_c^\pm + \Lambda_c I_{sol}, \quad (3.6)$$

where  $C_b$  and  $C_c$  are the heat capacities, and  $T_b(t)$  and  $T_c(t)$  are temperatures of the battery  $b$  and cabin  $c$  nodes respectively,  $H_{be}$ ,  $H_{bc}$ , and  $H_{ce}$  are the effective heat transfer coefficient between the battery, cabin, and ambient temperature  $e$  nodes,  $\Phi_b^\pm$  and  $\Phi_c^\pm$  are the battery thermal management and cabin A/C thermal power terms respectively,  $\Lambda_c$  is the effective surface area of the cabin, and finally  $I_{sol}$  is the solar irradiance. The values for the various parameters are presented in Tables 3.1 and 3.2.

In Eq. (3.5) the energy losses inside the battery are assumed to produce heat that affects the battery temperature node directly, whereas none of the energy losses in the on-board battery charger and the possible ICE are assumed to directly affect either the cabin or battery node temperatures. Effectively, this means that the vehicle is incapable of utilizing the waste heat from these components, which will unfortunately lead to the modelled PHEVs having slightly worse cold weather fuel efficiency than they would in reality. Utilizing the waste heat from the ICE would require

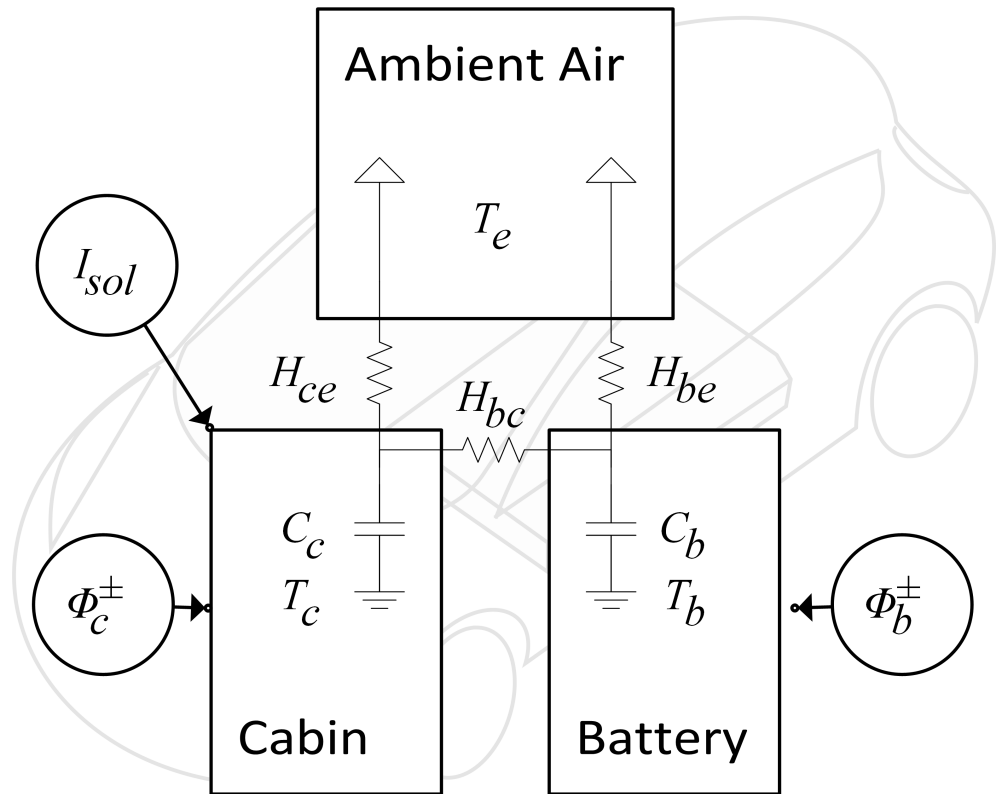


**Figure 3.7.** An illustration of the PEV thermal model.

some sort of additional variables that could dump the excess heat when it isn't useful, as otherwise the ICE overheats the cabin in the summer, complicating the computations.

Eqs. (3.5) and (3.6) can be cast into a linear form

$$\begin{bmatrix} \frac{dT_b(t)}{dt} \\ \frac{dT_c(t)}{dt} \end{bmatrix} = \begin{bmatrix} -\frac{H_{be}+H_{bc}}{C_b} & \frac{H_{bc}}{C_b} \\ \frac{H_{bc}}{C_c} & -\frac{H_{ce}+H_{bc}}{C_c} \end{bmatrix} \begin{bmatrix} T_b(t) \\ T_c(t) \end{bmatrix} + \begin{bmatrix} \frac{H_{be}T_e+\Phi_b^\pm+\dots}{C_b} \\ \frac{H_{ce}T_e+\Phi_c^\pm+\dots}{C_c} \end{bmatrix}, \quad (3.7)$$

and written as

$$\frac{d}{dt}\mathbf{x}(t) = \mathbf{A}\mathbf{x}(t) + \mathbf{b}, \quad (3.8)$$

where  $\mathbf{x}(t)$  is the node temperature vector,  $\mathbf{A}$  is a coefficient matrix, and  $\mathbf{b}$  is a vector containing the ambient temperature and power terms. Again, the various power terms are treated as hourly averages and assumed to stay constant over a single time step of  $\Delta t = 1$  h. Since the determinant of  $\mathbf{A}$  is non-zero as seen from Eq. (3.7), and thus  $\mathbf{A}$  is invertible, Eq. (3.8) can be solved and written using time step indexing as

$$\mathbf{x}_{t+1} - e^{\mathbf{A}\Delta t}\mathbf{x}_t = -(\mathbf{I} - e^{\mathbf{A}\Delta t})\mathbf{A}^{-1}\mathbf{b}_t. \quad (3.9)$$

The detailed derivation of the solution to a linear differential equation system in the form of Eq. (3.8) is presented in Appendix A. Eq. (3.9) can be written as

$$\begin{bmatrix} T_{b,t+1} \\ T_{c,t+1} \end{bmatrix} - \beta \begin{bmatrix} T_{b,t} \\ T_{c,t} \end{bmatrix} = -\gamma \begin{bmatrix} \frac{H_{be}T_{e,t}+\Phi_{b,t}^\pm+\dots}{C_b} \\ \frac{H_{ce}T_{e,t}+\Phi_{c,t}^\pm+\dots}{C_c} \end{bmatrix}, \quad (3.10)$$

where  $\beta = e^{\mathbf{A}\Delta t}$  and  $\gamma = (\mathbf{I} - e^{\mathbf{A}\Delta t})\mathbf{A}^{-1}$ . Using the coefficient matrices  $\beta$  and  $\gamma$ , we can write Eq. (3.10) as two separate equations again

$$\begin{aligned} T_{b,t+1} - \beta_{11}T_{b,t} - \beta_{12}T_{c,t} &= -\frac{\gamma_{12}}{C_c} [H_{ce}T_{e,t} + \Phi_{c,t}^\pm + \Lambda_c I_{sol,t}] \\ &\quad - \frac{\gamma_{11}}{C_b} [H_{be}T_{e,t} + \Phi_{b,t}^\pm + (1 - \eta_b)(\eta_c P_t^+ + P_t^- + \eta_F \eta_c F_{c,t}^+ + D_t^-)] \end{aligned} \quad (3.11)$$

$$\begin{aligned} T_{c,t+1} - \beta_{21}T_{b,t} - \beta_{22}T_{c,t} &= -\frac{\gamma_{22}}{C_c} [H_{ce}T_{e,t} + \Phi_{c,t}^\pm + \Lambda_c I_{sol,t}] \\ &\quad - \frac{\gamma_{21}}{C_b} [H_{be}T_{e,t} + \Phi_{b,t}^\pm + (1 - \eta_b)(\eta_c P_t^+ + P_t^- + \eta_F \eta_c F_{c,t}^+ + D_t^-)] \end{aligned} \quad (3.12)$$

where  $\beta_{ij}$  and  $\gamma_{ij}$  correspond to the elements of matrices  $\beta$  and  $\gamma$  on row  $i$  and column  $j$  respectively.

The thermal power terms  $\Phi_{b,t}^\pm$  and  $\Phi_{c,t}^\pm$  consist of different terms for the heating and cooling elements as follows

$$\Phi_{b,t}^\pm = \alpha_b^+ \psi_{b,t}^+ - \alpha_b^- \psi_{b,t}^-, \quad (3.13)$$

$$\Phi_{c,t}^\pm = \alpha_c^+ \psi_{c,t}^+ - \alpha_c^- \psi_{c,t}^-, \quad (3.14)$$



where  $\alpha_b^+$ ,  $\alpha_c^+$ ,  $\alpha_b^-$  and  $\alpha_c^-$  are the battery and cabin heating (+) and cooling (-) element coefficients of performance (COPs), and  $\psi_{b,t}^+$ ,  $\psi_{c,t}^+$ ,  $\psi_{b,t}^-$  and  $\psi_{c,t}^-$  are the corresponding heating element power draws. Typically such heating elements are simple electric heaters and pumps or fans associated with forced air or liquid cooling systems [40, 47, 32], and are approximated to have a constant COP for simplicity. The heating element power draws in Eqs. (3.13) and (3.14) are connected to the total BMS and vehicle A/C power draw term  $\Psi^\pm$  in Eq. (3.4) via

$$\Psi_t^\pm = \psi_{b,t}^+ + \psi_{b,t}^- + \psi_{c,t}^+ + \psi_{c,t}^- \quad (3.15)$$

The values for the heat transfer coefficients and the cabin heat capacity are obtained from [40, 50], where a similar thermal model was fit into experimental data recorded for a *2005 Toyota Prius*, and used to study the impact of thermal management in a BEV on its utility. Similarly to the energy dynamics, the assumption of the power terms staying constant during the hourly time step is rather unrealistic, which will be discussed further in Section 5.1.

**Table 3.1.** Car-independent parameters used for the PEV modelling.

Symbol	Description	Value
$\nu$	Hourly battery self-discharge rate	$10^{-4} \frac{1}{h}$ [33]
$\psi_{max,b,v}^+$	Battery heating element max power	300 W [40]
$\psi_{max,b,v}^-$	Battery cooling element max power	1400 W [40]
$\psi_{max,c,v}^+$	Cabin heating element max power	4000 W [40]
$\psi_{max,c,v}^-$	Cabin cooling element max power	1800 W [40]
$\alpha_b^+$	Battery heating element COP (PTC heater)	1 [40]
$\alpha_b^-$	Battery cooling element COP (liquid cooled)	2.5 [40]
$\alpha_c^+$	Cabin heating element COP (PTC heater)	1 [40]
$\alpha_c^-$	Cabin cooling element COP (A/C)	2.5 [40]
$C_c$	Cabin heat capacity	$28.3 \frac{Wh}{K}$ [50]
$H_{ce}$	Heat transfer coefficient	$22.6 \frac{Wh}{K}$ [50]
$\Lambda_c$	Effective cabin surface area	$0.77 \text{ m}^2$ [50]
$T_{max,c}$	Maximum driving cabin temperature	$24^\circ\text{C}$ [48]
$T_{min,c}$	Minimum driving cabin temperature	$16^\circ\text{C}$ <sup>a</sup>
$T_{max,b}$	Maximum battery temperature	$50^\circ\text{C}$ [33]
$T_{min,b}$	Minimum off-grid battery temperature	$-17^\circ\text{C}$ [33]

<sup>a</sup>Around  $22^\circ\text{C}$  in [48], excessive when passengers are appropriately clothed.

**Table 3.2.** Car-dependent parameters used for the PEVs modelled in this work.

Symbol	Description	2013 Chevrolet Volt (PHEV)	2013 Nissan Leaf (BEV)	High-End BEV <sup>a</sup>
$E_{max,v,0}$	Nominal battery capacity	16.5 kWh [47]	24.0 kWh [47]	70 kWh [51]
$Q_{battery}$	Nominal battery Ah-capacity	45.0 Ah [47]	66.2 Ah [47]	193.1 Ah
$SOC_{min}$	Minimum allowed battery SOC <sup>b</sup>	0.13 [47]	0.10 [47]	0.1
$U$	Nominal battery voltage	355.2 V [47]	364.8 V [47]	366.0 V [51]
$\eta_b$	Battery efficiency <sup>c</sup>	$\sqrt{0.98}$ [47]	$\sqrt{0.98}$ [47]	$\sqrt{0.98}$
$\eta_c$	On-board charger efficiency	0.91 [47]	0.87 [47]	0.87
$\eta_F$	ICE energy conversion efficiency	0.3 [52]	0	0
$P_{max,v}^{\pm}$	On-board charger max. power	3.1 kW [48]	6.7 kW [48]	11.0 kW [53]
$F_{max,v}^+$	Fuel charging max. power	111 kW [47]	0 kW	0 kW
$C_b$	Battery heat capacity	$43.57 \frac{\text{Wh}}{\text{K}}$ [47, 54]	$64.11 \frac{\text{Wh}}{\text{K}}$ [47, 54]	$185.9 \frac{\text{Wh}}{\text{K}}$
$H_{be}$	Heat transfer coefficient	$1.049 \frac{\text{W}}{\text{K}}$ [50]	$4.343 \frac{\text{W}}{\text{K}}$ [50]	$12.60 \frac{\text{W}}{\text{K}}$
$H_{bc}$	Heat transfer coefficient	$0.752 \frac{\text{W}}{\text{K}}$ [50]	$3.468 \frac{\text{W}}{\text{K}}$ [50]	$10.06 \frac{\text{W}}{\text{K}}$
	UDDS driving consumption	$157.6 \frac{\text{Wh}}{\text{km}}$ [47]	$125.1 \frac{\text{Wh}}{\text{km}}$ [47]	$170.4 \frac{\text{Wh}}{\text{km}}$

<sup>a</sup>The *High-End BEV* is loosely based on the *Tesla Model S*, as necessary technical specifications were not found to model the original Model S properly, and parameters lacking a reference were scaled from *Nissan Leaf* parameters according to vehicle weight ratio or battery size ratio.

<sup>b</sup>The minimum SOC values are low enough to affect the driving performance of the modelled vehicles [47], but are required for the *Nissan Leaf* to manage through the winter with the modelled driving patterns.

<sup>c</sup>The square root of the battery efficiency is used, because the losses are applied equally when both charging and discharging the battery.

### Battery Ageing Model

For V2G purposes, the capability to estimate the capacity fade of the batteries due to possibly irregular charging and discharging patterns is helpful, as it allows us to estimate the costs associated with V2G use. For this purpose, we employ a cycle-life ageing model proposed by A. Cordoba-Arenas *et al.* [55]

$$L(t) = a_c \exp\left(-\frac{E_{ac}}{R_g T_{cell}}\right) j(t)^z, \quad (3.16)$$

$$\text{where } a_c = \alpha_c + \beta_c r^b + \gamma_c (SOC_{min} - SOC_0)^c.$$

$L(t)$  is the cumulative cell capacity fade percentage at time  $t$ ,  $r$  is a parameter that determines whether the vehicle is driven in charge-depleting (CD) or charge-sustaining (CS) mode,  $SOC_{min}$  is the minimum permitted SOC of the battery cell,  $E_{ac}$  is the cell activation energy for the capacity fade process,  $R_g$  is the universal gas constant,  $T_{cell}$  is the surface temperature of the cell, and  $j(t)$  is the Ah throughput in both charge and discharge. The terms  $\alpha_c$ ,  $\beta_c$ ,  $b$ ,  $\gamma_c$ ,  $SOC_0$ ,  $c$ , and  $z$  are dimensionless coefficients used in fitting the model to the experimental data from a 15 Ah 3.75 V NMC-LMO/Graphite cell, presented in Table 3.3. This cell chemistry is a slower degrading improvement on the LMO/Carbon cells that are actually used in the modelled PEVs [55], and is used because sufficiently accurate ageing models for LMO/Carbon cells couldn't be found in literature.

CD and CS modes are terms used with PHEVs, and correspond to how the battery and ICE are used together. In CD mode the PHEV operates the ICE in a way that results in the SOC of the battery system decreasing,

**Table 3.3.** The various parameters used in the capacity fade model [55].

Symbol	Description	Value
$E_{ac}$	Cell capacity fade process activation energy	22,406 $\frac{\text{J}}{\text{mol}}$
$R_g$	Universal gas constant	8.314 $\frac{\text{J}}{\text{K mol}}$
$r$	Driving mode parameter	1
$\alpha_c$	Model fitting parameter	137
$\beta_c$	Model fitting parameter	420
$\gamma_c$	Model fitting parameter	9610
$b$	Model fitting parameter	0.34
$c$	Model fitting parameter	3
$z$	Model fitting parameter	0.48
$SOC_0$	Model fitting parameter	0.25

meaning that the ICE generates less electricity than the PHEV consumes, if any at all. In CS mode the PHEV keeps the SOC of the battery constant using the ICE. For simplicity, we assume the PHEV to operate in CD mode whenever possible, resulting in  $r = 1$  for both the BEV and the PHEV. [55]

The model in Eq. (3.16) doesn't allow for changing cell temperature, but an approximation can be derived using the first order Taylor expansion

$$L(t + \Delta t) \approx L(t) + \frac{dL(t)}{dj(t)} \Delta j(t),$$

which can be resolved as

$$L_{t+1} = L_t + za_c \exp\left(-\frac{2E_{ac}}{R_g(T_{cell,t+1} + T_{cell,t})}\right) j_t^{z-1} (j_{t+1} - j_t), \quad (3.17)$$

using time step indexing. Since in reality the temperature of the cells is changing during the time step, we calculate the battery degradation by using the mean temperature during the step. This is done in order to account for the rising battery temperatures during driving, charging, and discharging of the battery system, discussed further in Section 5.1.

As Eq. (3.17) is still formulated for a single cell, we need to adjust the Ah throughput through each cell to match the throughput of the whole battery system. In a battery system, the total Ah capacity is determined by the parallel connected cell stacks. Assuming an ideal BMS that ensures all the cells are drained equally and their temperatures are equalized, we can write

$$j(t) = \frac{Q_{cell}}{Q_{battery}} J(t),$$

which can be substituted into Eq. (3.17) resulting in

$$L_{t+1} = L_t + za_c \left(\frac{Q_{cell}}{Q_{battery}}\right)^z \exp\left(-\frac{2E_{ac}}{R_g(T_{b,t+1} + T_{b,t})}\right) J_t^{z-1} (J_{t+1} - J_t), \quad (3.18)$$

where  $Q_{cell}$  and  $Q_{battery}$  are the rated Ah capacities of the individual battery cell and the battery system respectively, and  $J_t$  is the Ah throughput of the battery system at time step  $t$ , defined as [55]

$$J(t) = \int_0^t |I(t)| dt = \int_0^t \left| \frac{P(t)}{U(t)} \right| dt,$$

where  $I(t)$  is the total current to or from the battery. For our purposes, this is approximated as

$$J_t \approx \frac{1}{U} \sum_1^t \eta_c (P_t^+ + \eta_F F_t^+) + P_t^- + D_t^- + \Psi_t^\pm, \quad (3.19)$$

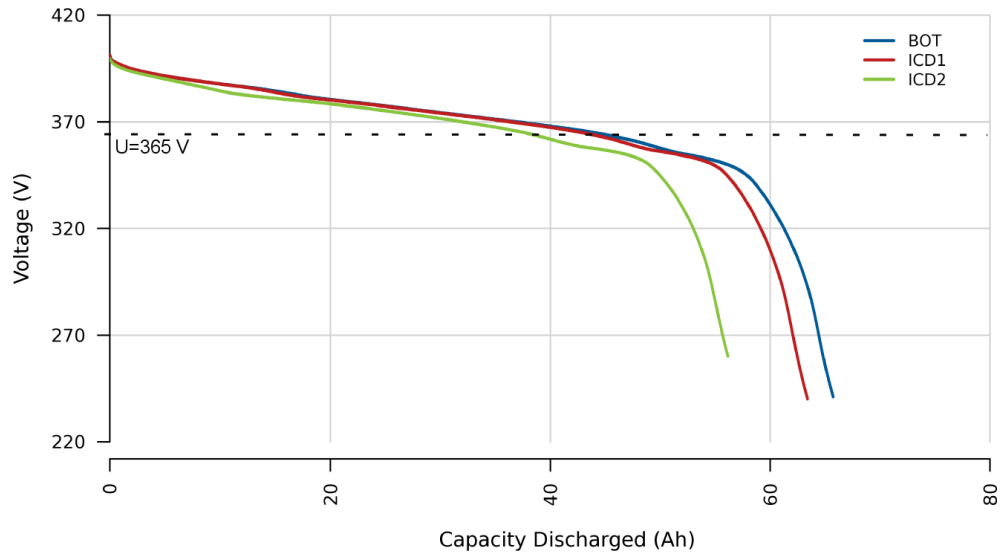


**Figure 3.8.** Measured *Nissan Leaf* VIN 7885 battery system voltages as a function of discharged Ah capacity. *BOT* is a baseline corresponding to 562 miles driven, *ICD1* a later measurement with 4,813 miles driven, and *ICD2* the latest measurement with 15,736 miles driven. Graph from [47] with added line denoting the nominal battery voltage  $U$ .

where  $U$  is the nominal voltage of the battery system. Eqs. (3.18) and (3.19) now allow us to calculate the battery capacity loss percentage  $L_t$ , as long as the time series  $J_t$  and  $T_{b,t}$  are known.

In reality, the PEV battery system voltage decreases as the SOC of the battery goes down, as can be seen from Figure 3.8, which affects the Ah throughput. The capacity fade model in Eq. (3.18) was tested with a linear approximation between the battery system voltage and discharged capacity to better account for the changes in voltage, and both models were compared to the original model in Eq. (3.16) in a scenario measured in [55]. The model with SOC-dependent linear voltage resulted in battery degradation more similar to the results of the original model, but only when the computational steps were sufficiently small. With computational steps comparable to the hourly time scale used in the intended simulations however, the model using the nominal battery system voltage better reproduces the results of the original battery model, and is therefore used in this work.

### 3.3 Space Heating Load

The thermal modelling of the detached houses is done using a two-capacity model similar to that of the PEVs, illustrated in Figure 3.9. According to the *TABULA* national building typologies [56], typical single-family houses in southern Sweden have rather light wooden structures, except for a concrete slab floor. Since the floor contains a significant portion of the total heat capacity of the house, it is separated into a dedicated temperature node apart from the rest of the house. The detached houses are assumed to have so called plinth foundations [57], allowing us to use the same external temperature time series for the heat losses through the floor as through the rest of the house exterior. This type of foundations slightly increases the overall heat losses of the detached houses, but avoids the need to model the complex interaction between the ground and the floor.

The energy balance equations for the interior and floor nodes can be written as

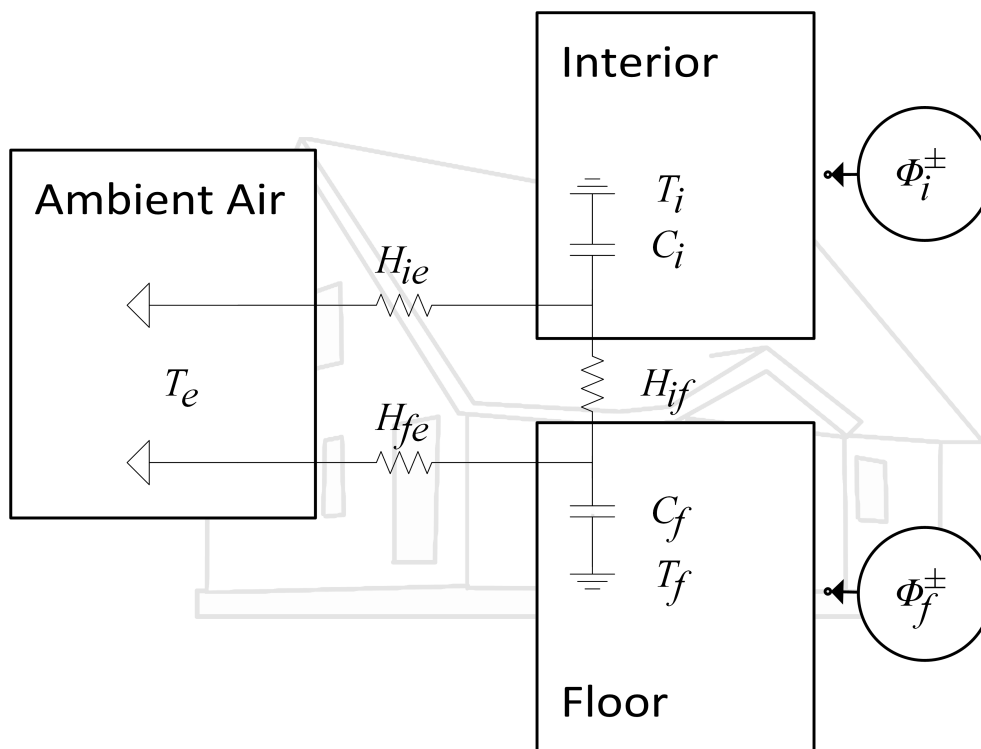


**Figure 3.9.** An illustration of the detached house thermal model. The concrete floor slab is modelled as a separate temperature node while the walls, roof, and inside air are lumped together into a single temperature node representing the rest of the house.

$$C_i \frac{dT_i}{dt} = \Phi_i^\pm + H_{ie}(T_e - T_i) + H_{if}(T_f - T_i), \quad (3.20)$$

$$C_f \frac{dT_f}{dt} = \Phi_f^\pm + H_{fe}(T_e - T_f) + H_{if}(T_i - T_f), \quad (3.21)$$

where  $C_i$  and  $C_f$  are the heat capacities,  $T_i$  and  $T_f$  are the temperatures, and  $\Phi_i^\pm$  and  $\Phi_f^\pm$  are the thermal power terms to the interior  $i$  and floor  $f$  nodes respectively.  $H_{ie}$ ,  $H_{if}$ , and  $H_{fe}$  are the heat transfer coefficients between the interior, floor, and ambient air  $e$  nodes. Eqs. (3.20) and (3.21) can be expressed in a linear form

$$\begin{bmatrix} \frac{dT_i}{dt} \\ \frac{dT_f}{dt} \end{bmatrix} = \begin{bmatrix} -\frac{H_{ie}+H_{if}}{C_i} & \frac{H_{if}}{C_i} \\ \frac{H_{if}}{C_f} & -\frac{H_{fe}+H_{if}}{C_f} \end{bmatrix} \begin{bmatrix} T_i \\ T_f \end{bmatrix} + \begin{bmatrix} \frac{\Phi_i^\pm + H_{ie}T_e}{C_i} \\ \frac{\Phi_f^\pm + H_{fe}T_e}{C_f} \end{bmatrix}, \quad (3.22)$$

and written as

$$\frac{d}{dt}\mathbf{y}(t) = \mathbf{B}\mathbf{y}(t) + \mathbf{c}, \quad (3.23)$$

where  $\mathbf{y}(t)$  is the temperature vector,  $\mathbf{B}$  is the coefficient matrix and  $\mathbf{c}$  is a vector containing the thermal power terms and the effects of the external temperature. Since Eq. (3.23) is identical in form to Eq. (3.8) and  $\mathbf{B}$  is invertible, it can be solved as shown in Appendix A resulting in

$$\mathbf{y}_{t+1} - e^{\mathbf{B}\Delta t}\mathbf{y}_t = -(\mathbf{I} - e^{\mathbf{B}\Delta t})\mathbf{B}^{-1}\mathbf{c}_t, \quad (3.24)$$

when using time step indexing. Since each house has different thermal properties, each house  $h$  has a different coefficient matrix  $\mathbf{B}_h$ . Denoting  $e^{\mathbf{B}_h\Delta t} = \epsilon_h$  and  $(\mathbf{I} - e^{\mathbf{B}_h\Delta t})\mathbf{B}_h^{-1} = \zeta_h$ , Eq. (3.24) becomes

$$\mathbf{y}_{h,t+1} - \epsilon_h\mathbf{y}_{h,t} = -\zeta_h\mathbf{c}_{h,t}, \quad \forall h, t$$

which can be written as two separate equations for the interior and floor node temperatures

$$T_{i,h,t+1} - \epsilon_{h,11}T_{i,h,t} - \epsilon_{h,12}T_{f,h,t} = -\frac{\zeta_{h,11}}{C_{i,h}}(\Phi_{i,h,t}^\pm + H_{ie,h}T_{e,t}) - \frac{\zeta_{h,12}}{C_{f,h}}(\Phi_{f,h,t}^\pm + H_{fe,h}T_{e,t}) \quad \forall h, t \quad (3.25)$$

$$T_{f,h,t+1} - \epsilon_{h,21}T_{i,h,t} - \epsilon_{h,22}T_{f,h,t} = -\frac{\zeta_{h,21}}{C_{i,h}}(\Phi_{i,h,t}^\pm + H_{ie,h}T_{e,t}) - \frac{\zeta_{h,22}}{C_{f,h}}(\Phi_{f,h,t}^\pm + H_{fe,h}T_{e,t}) \quad \forall h, t \quad (3.26)$$

where  $\epsilon_{h,jk}$  and  $\zeta_{h,jk}$  are the elements of the coefficient matrices  $\epsilon_h$  and  $\zeta_h$  of house  $h$ , on row  $j$  and column  $k$ .

In a study by *K. K. Andersen et al.* [58], the direct solar radiation into the test room was found to only directly affect the inside air temperature instead of the temperature of the floor. This is likely due to the thermal radiation being absorbed by the immediate surface of the floor, from which the heat is quickly transferred into the inside air via convection. This is assumed to also apply to any thermal radiation from the radiator system, meaning that no thermal power terms have a significant direct effect on the mass node temperature when using radiators for space heating. For a radiator system, the thermal power terms can now be broken down as follows

$$\begin{aligned}\Phi_{i,h,t}^{\pm} &= \alpha_{h,t}^+ P_{h,t}^+ - \alpha_{h,t}^- P_{h,t}^- + P_{app,h,t} + \varphi_{ppl,h,t} + \varphi_{sol,h,t} \\ \Phi_{f,h,t}^{\pm} &= 0\end{aligned}\quad \forall h, t, \quad (3.27)$$

where  $\alpha_{h,t}^+$  is the COP and  $P_{h,t}^+$  is the power draw of the heating equipment in house  $h$  on time step  $t$ ,  $\alpha_{h,t}^-$  is the COP and  $P_{h,t}^-$  is the power draw of the cooling equipment,  $P_{app,h,t}$  is the total power consumption of all the appliances and lights in house  $h$ ,  $\varphi_{ppl,h,t}$  is the passive heating power of the residents, and  $\varphi_{sol,h,t}$  are the passive solar heat gains. For a radiant floor heating system, the power terms can be written

$$\begin{aligned}\Phi_{i,h,t}^{\pm} &= -\alpha_{h,t}^- P_{h,t}^- + P_{app,h,t} + \varphi_{ppl,h,t} + \varphi_{sol,h,t} \\ \Phi_{f,h,t}^{\pm} &= \alpha_{h,t}^+ P_{h,t}^+\end{aligned}\quad \forall h, t. \quad (3.28)$$

All the electricity consumed by the household appliances and lighting is assumed to turn into heat within the house eventually.

The *SEA* data does contain electricity consumed by heating loads in the households, but not all the measured households were primarily heated with electricity. Other forms of space heating or heating of DHW, such as district heating, aren't visible from electricity consumption measurements. Fortunately, the *SEA* data contains information on the floor areas and building years of each household, as well as the number of inhabitants, allowing us to model the space heating and DHW systems separately using *TABULA* [56] building typologies for the thermal parameters of each house. The passive heating power of the residents is calculated from a typical daily schedule according to Swedish statistics from 1990/91 [59] and average heat gains of the different activities [60]. Newer statistics from 2010/11 [61] don't present an applicable average daily schedule, but tell us that there are no changes from the 1990/91 survey that are significant on an hourly time scale. The passive solar heat gains were calculated with *ALLSOL* [62] by *SOLPROS*.



The thermal parameters of the houses are estimated assuming that they are rectangular and single-storey. The floor node heat capacity  $C_{f,h}$  for each house  $h$  is calculated as the heat capacity of the concrete slab covering the total floor area of the house, and the interior node heat capacity is calculated using the floor heat capacity as follows

$$C_{f,h} = c_c z_f A_{fl,h}, \quad (3.29)$$

$$C_{i,h} = C_{ref} A_{fl,h} - C_{f,h}, \quad (3.30)$$

where  $c_c$  is the volumetric specific heat capacity of concrete,  $z_f$  is the thickness of the floor slab,  $A_{fl,h}$  is the floor surface area of house  $h$ , and  $C_{ref}$  is the *TABULA* reference heat capacity of a typical single family house in southern Sweden built between 1976 and 1985 [56] with advanced refurbishment. Floor slab thickness of  $z_f = 8$  cm is found to be reasonable considering the *TABULA* reference heat capacity, as well as typical underfloor heating system floor slab thickness of around 10 cm [63].

The heat transfer coefficients between the temperature nodes are calculated for each house  $h$  as follows [56, 64]

$$H_{if,h} = \bar{v} A_{fl,h}, \quad (3.31)$$

$$H_{fe,h} = \left[ \left( \frac{1}{U_{fl}} - \frac{1}{\bar{v}} \right)^{-1} + \Delta U_{tb} \right] A_{fl,h}, \quad (3.32)$$

$$H_{ie,h} = c_a \mu h_{wa} A_{fl,h} + \sum_{p \in S_m} [(U_p + \Delta U_{tb}) A_{p,h}], \quad S_m = \{wi, do, ro, wa\} \quad (3.33)$$

where  $\bar{v}$  is the mean total heat transfer factor between the floor and the interior nodes,  $U_p$  is the *TABULA* reference U-value of structural part  $p$  of house  $h$ ,  $A_{p,h}$  is the approximated surface area,  $\Delta U_{tb}$  is the extra heat transfer due to thermal bridging,  $c_a$  is the volumetric specific heat capacity of air at 20°C,  $\mu$  is the *TABULA* reference air exchange rate, and  $h_{wa}$  is the minimum residential dwelling room height [65]. The different structural parts  $p$  in set  $S_m$  are denoted with sub-indexes: windows  $wi$ , doors  $do$ , roof  $ro$ , and walls  $wa$ . Values of the various parameters used in the thermal modelling of the detached houses are presented in Tables 3.4 and 3.5.

The mean total heat transfer factor between the floor and the interior  $\bar{v}$  was determined based on a study by *T. Cholewa et al.* [66], who proposed

$$v(T_s, T_{op1.1}) = 7.67(T_s - T_{op1.1})^{0.1} \quad (3.34)$$

for radiant floor heating systems, where  $T_s$  is the surface temperature of the floor, and  $T_{op1.1}$  is the operative temperature in the room at the height of 1.1 m. Operative temperature is defined as the average of the mean radiant temperature of the surrounding surfaces and the temperature of the air [63]. Since the two-capacity thermal model assumes homogeneous temperatures inside the nodes, Eq. (3.34) can be approximated as

$$v(T_{f,h,t}, T_{i,h,t}) \approx 7.67(T_{f,h,t} - T_{i,h,t})^{0,1}. \quad (3.35)$$

**Table 3.4.** House related parameters used in the thermal modelling of the detached houses [43]. The *door*, *window*, *roof* and *wall* areas are estimated based on known floor areas and *TABULA* [56] reference house measurements. The *Norm.* house is used for simulations with normalized yearly electricity consumption.

Name	$N_{ppl,h}$	$A_{fl}$ [m <sup>2</sup> ]	$A_{wi}$ [m <sup>2</sup> ]	$A_{do}$ [m <sup>2</sup> ]	$A_{ro}$ [m <sup>2</sup> ]	$A_{wa}$ [m <sup>2</sup> ]
House 1	5	191	33.6	2.77	191	138
House 2	2	200	35.2	2.82	200	141
House 3	2	155	27.3	2.48	155	124
House 4	2	164	28.9	2.56	164	127
House 5	2	140	24.6	2.36	140	118
Norm.	2.7	170	29.9	2.60	170	130

**Table 3.5.** Parameters used in the thermal modelling of the detached houses. *TABULA* [56] reference values from a typical climatic zone 3 (southern Sweden) single-family house built between 1976-1985 with advanced refurbishment.

Symbol	Description	Value
$c_c$	Volumetric heat capacity of concrete	490 $\frac{\text{Wh}}{\text{Km}^3}$ [63]
$c_a$	Volumetric heat capacity of air at 20°C	0.34 $\frac{\text{Wh}}{\text{Km}^3}$ [64]
$z_f$	Floor slab thickness	0.08 m [63]
$\bar{v}$	Mean floor-interior heat transfer factor	7.70 $\frac{\text{W}}{\text{Km}^2}$
$h_{wa}$	Minimum residential dwelling room height	2.4 m [65]
$C_{ref}$	Reference heat capacity of a typical house	45 $\frac{\text{Wh}}{\text{Km}^2}$ [56]
$\mu$	Reference air exchange rate	0.60 $\frac{1}{\text{h}}$ [56]
$U_{wi}$	Reference window U-value	0.76 $\frac{\text{W}}{\text{Km}^2}$ [56]
$U_{do}$	Reference door U-value	0.90 $\frac{\text{W}}{\text{Km}^2}$ [56]
$U_{fl}$	Reference floor U-value	0.20 $\frac{\text{W}}{\text{Km}^2}$ [56]
$U_{ro}$	Reference roof U-value	0.05 $\frac{\text{W}}{\text{Km}^2}$ [56]
$U_{wa}$	Reference walls U-value	0.15 $\frac{\text{W}}{\text{Km}^2}$ [56]
$\Delta U_{tb}$	Extra heat transfer due to thermal bridging	0.10 $\frac{\text{W}}{\text{Km}^2}$ [56]

The thermal model cannot explicitly account for Eq. (3.35) without becoming non-linear, so in this work we calculate  $\bar{v}$  using the mean temperatures  $\bar{T}_{f,h,t}$  and  $\bar{T}_{i,h,t}$ , resulting in  $\bar{v} \approx 7.7 \frac{\text{W}}{\text{Km}^2}$ . This heat transfer factor is also used for the heat transfer between the floor and interior when modelling a radiator system instead of a radiant floor heating system, even though the difference in the mean temperatures  $\bar{T}_{f,h,t}$  and  $\bar{T}_{i,h,t}$  is slightly smaller. However, based on a few tests the overall performance of the heating system is barely affected by small ( $\approx \pm 2.0 \frac{\text{W}}{\text{Km}^2}$ ) changes in the mean heat transfer coefficient  $\bar{v}$ .

### *HVAC System*

The houses in the MG are modelled to have a hydronic heating system with a ground source heat pump for both heating and cooling. Hot water heated with the heat pump is circulated through the radiators or the floor heating system to provide heating when necessary, whereas cold water from the borehole is circulated through heat exchangers located in the air exchange channels to provide cooling. Cooling the house this way is extremely efficient, only requiring the use of circulation pumps and fans. This type of system is modelled in this work as having a maximum electric power draw of  $P_{max,h}^- = 300 \text{ W}$  corresponding to typical ventilation equipment power draws measured in the *SEA* data, with a constant COP of  $\alpha_{ac}^- = 30$  approximated to be equal to the seasonal energy efficiency ratio typical of such systems [67]. The modelled heating system is illustrated in Figure 3.10.

The supply and return temperatures of hydronic heating systems are adjusted according to external temperature to ensure sufficient heating [64], which affects the COP of the heat pump. In this work, the heating system supply temperature  $T_{sup,t}$  is approximated as a linear function of the external temperature as

$$T_{sup,t} = \tau - \kappa T_{e,t}, \quad T_{e,t} \leq 20^\circ\text{C} \quad (3.36)$$

$$T_{sup,t} = 25^\circ\text{C}, \quad T_{e,t} > 20^\circ\text{C} \quad (3.37)$$

where  $\tau$  K and  $\kappa$  are coefficients that depend on the type of hydronic heating system used. The minimum supply temperature is set to  $25^\circ\text{C}$  in order to always allow the houses to be heated.

For a radiator system with sufficient oversizing, the supply and return temperatures at  $-15^\circ\text{C}$  external temperature can be lowered to  $55/45^\circ\text{C}$ , instead of the typical  $80/60^\circ\text{C}$  systems without oversizing in Sweden [68]. For radiant floor heating systems the supply temperatures can be kept

lower due to larger surface area of the floor compared to that of the radiators, with typically around  $35^{\circ}\text{C}$  supply temperature at  $-15^{\circ}\text{C}$  external temperature [64]. The heating system supply temperature coefficients according to Eq. (3.37) for both radiator and floor heating are presented in Table 3.6, along with heat pump related parameters.

The temperature dependent COP of the heat pump  $\alpha_{hp,t}^+$  can be modelled using the COP of a corresponding ideal Carnot heat pump cycle [71, 70]

$$\alpha_{hp,t}^+ = \eta_{Ca} \frac{T_g - \delta T}{T_{sup,t} - T_g + 2\delta T} + 1, \quad (3.38)$$

where  $T_g$  is the yearly average temperature of the ground heat source,  $\eta_{Ca}$  is the Carnot efficiency, and  $\delta T$  is the temperature difference of the heat exchangers. For ground source heat pumps, parameter values of  $\eta_{Ca} = 0.55$  [70] and  $\delta T = 5^{\circ}\text{C}$  [71] are considered reasonable. Since the heat pump output temperature is assumed to be fixed to the supply water temperature of the heating system, this effectively means that the heating power is assumed to be controlled solely by adjusting the speed of the circulation pumps. In reality, such a system might require specialized dimensioning of the floor heating systems.

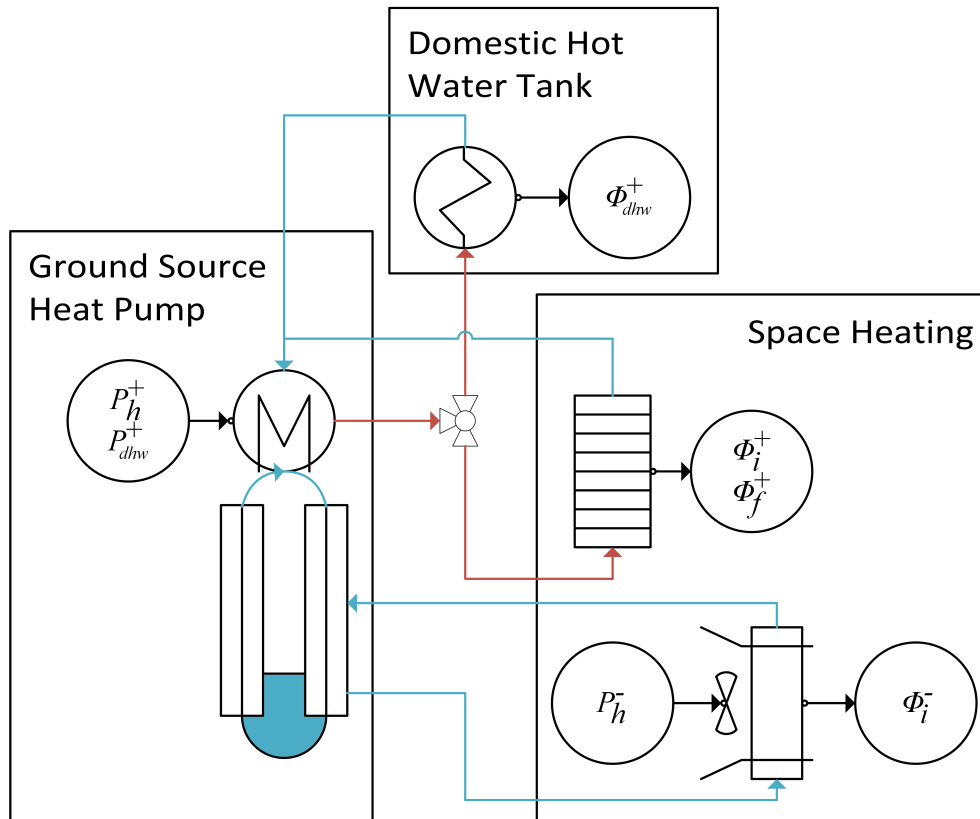


**Figure 3.10.** An illustration of the modelled hydronic heating system with a ground source heat pump for both space and DHW heating. Cooling is done by circulating cold water from the borehole through heat exchangers in the ventilation, sometimes called ground source free cooling.

**Table 3.6.** Values of the various parameters used in the modelling of the HVAC system.

Symbol	Description	Value
$\tau_{rad}$	Radiator supply temperature parameter	549.4214 K
$\kappa_{rad}$	Radiator supply temperature parameter	-0.8571
$\tau_{r,fh}$	Floor heating supply temperature parameter	381.9071 K
$\kappa_{r,fh}$	Floor heating supply temperature parameter	-0.2857
$P_{max,h}^+$	Heat pump maximum electric power	6 kW [69]
$\eta_{Ca}$	Carnot efficiency parameter of the heat pump	0.55 [70]
$\delta T$	Heat exchanger temperature difference	5 K [71]
$T_g$	Yearly average borehole water temperature	1°C [72]
$P_{max,h}^-$	Cooling equipment maximum electric power	300 W
$\alpha_{ac}^-$	Ground source free cooling COP	30 [67]
$T_{max,i}$	Maximum interior node temperature	22°C [43]
$T_{min,i}$	Minimum interior node temperature	20°C [43]
$T_{max,f}$	Maximum floor node temperature	29°C [73]
$T_{min,f}$	Minimum floor node temperature	19°C [73]

### Domestic Hot Water

DHW is a significant heat load for residential houses, and one which isn't included in every house of the *SEA* electricity consumption data. As illustrated in Figure 3.10 the heating of DHW is done using the same ground source heat pump that is connected to the space heating system using a switching valve. Swedish regulations from 2006 demand that DHW must be heated to between 50–60°C to minimize the risks of bacterial contamination and accidental scalding [74]. In this work the DHW storage tank is modelled as fully mixed for simplicity, and combined with the predetermined consumption of DHW the total energy flexibility of a 180 l DHW storage tank only amounts to around 2 kWh. This is rather small compared to the flexibility offered by the PEV batteries or the thermal mass of the houses (>10 kWh), and therefore the DHW storage tank is not dispatched in the model. However, heating DHW still affects the operation of the heat pump.

Because the temperature of the tank is kept constant, the thermal power required for the DHW is

$$\phi_{dhw,t} = V_{dhw,t}(c_{dhw}T_{dhw} - c_{in}T_{in}) + H_{dhw}(T_{dhw} - T_{max,i}), \quad (3.39)$$

where  $V_{dhw,t}$  is the volume of used DHW per person on hour  $t$ ,  $c_{dhw}$  and  $c_{in}$  are the specific heat capacities of the hot water and cold inlet water

respectively,  $T_{dhw}$  and  $T_{in}$  are the temperatures of the hot water and cold inlet water respectively,  $H_{dhw}$  is the heat transfer coefficient between the DHW tank and its surroundings, and  $T_{max,i}$  is the ambient temperature surrounding the tank, approximated here as the maximum permitted interior node temperature. DHW storage tanks in houses are usually located out of sight in areas that don't require the same level of thermal comfort as the living spaces. For simplicity, the ambient temperature surrounding the DHW tank is considered to remain constant, and not affected by the modelled interior temperature node of the house. Similarly, the heat losses from the DHW tank are considered not to affect the interior temperature node. Parameters related to the DHW modelling are presented in Table 3.7

The DHW consumption time series  $V_{dhw,t}$  is constructed using hourly average DHW use profiles for workdays and weekends separately [75]. These profiles are based on measurements by the *SEA* in the Stockholm area between October 2006 and June 2007 [76], scaled to match the average daily DHW consumption of Swedish one-family houses of 42 l per person [77].

**Table 3.7.** DHW related parameters. The storage tank is modelled as a cylinder with radius-to-height ratio of 1:3, a volume of 180 l, and a U-value of  $0.3 \frac{W}{Km^2}$  [78].

Symbol	Description	Value
$H_{dhw}$	Heat transfer coefficient to ambient air	$0.5387 \frac{W}{K}$
$T_{in}$	Inlet water temperature	$8^{\circ}C$ [79]
$T_{dhw}$	Required hot water temperature	$60^{\circ}C$ [74]
$c_{dhw}$	Specific heat capacity of water at $60^{\circ}C$	$1.14 \frac{kWh}{Km^3}$ [64]
$c_{in}$	Specific heat capacity of water at $8^{\circ}C$	$1.16 \frac{kWh}{Km^3}$ [64]
$\alpha_{dhw}^+$	Heat pump COP for DHW	3.14

### 3.4 Renewable Generation and Energy Prices

Hourly direct and diffuse solar irradiance measurements from the Norrköping-SMHI weather station ( $58.58^{\circ}N$   $16.15^{\circ}E$ ) were obtained through private communication with the *Swedish Meteorological and Hydrological Institute (SMHI)* [80]. The hourly solar electricity production in the MG, and the passive solar heat gains of the houses  $\varphi_{sol,h,t}$  were calculated using *ALLSOL* [62] by *SOLPROS*, with the modelled PV panels aligned southwards with a  $30^{\circ}$  inclination.

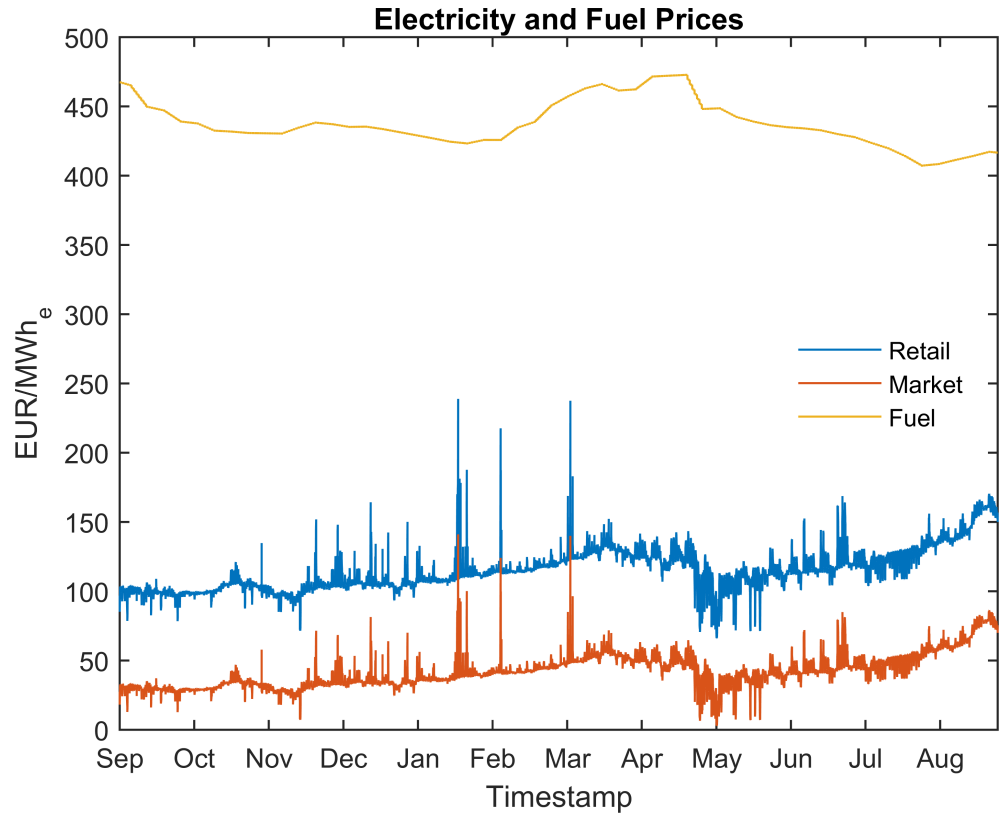


**Figure 3.11.** The retail and market prices of electricity as well as the price of fuel in  $\frac{\text{€}}{\text{MWh}}$  of electricity produced by the PHEV ICEs.

Hourly electricity spot market prices for the SE area in 2005–2006 were obtained from *Nord Pool Spot* [81]. The retail electricity prices  $p_{r,t}$  are calculated as

$$p_{r,t} = 1.25 \times (p_{m,t} + p_f), \quad \forall t \quad (3.40)$$

where the multiplier of 1.25 accounts for the value-added tax,  $p_{m,t}$  is the hourly spot market price, and  $p_f$  accounts for the additional fees for the consumer. Additional fees of  $p_f = 50 \frac{\text{€}}{\text{MWh}}$  are considered reasonable for an average Swedish customer [44]. Eq. (3.40) assumes no support schemes and that the surplus renewable electricity is sold to an electricity trader at the hourly spot market price. The retail and market electricity prices, as well as fuel prices, are presented in Figure 3.11.

Fuel price data was obtained from the *Weekly Oil Bulletin* statistics by the *European Energy Commission* [82]. The fuel prices used in this work are tax-inclusive EU weighted weekly average prices of *Euro-Super 95* petrol from 2005–2006, which were linearly interpolated to daily values that change at midnight, as is typical for gasoline stations. The energy content in the fuel is calculated with a typical energy density of gasohol E10 of about  $9.2 \frac{\text{kWh}}{\text{l}}$  [83], and the PHEV ICEs are assumed to have 30% energy conversion efficiency [52].

## 4. Linear Programming Formulation

In this work, the potential benefits of the V2G and utilizing building thermal mass for residential customers are assessed by modelling a small residential MG using LP methodology, and solving the cost optimal dispatch of the PEVs and the space heating load. The canonical formulation of a LP problem can be expressed as

$$\begin{aligned} \min \quad & \mathbf{f}^T \mathbf{z}, \\ \text{s.t.} \quad & \mathbf{M}_1 \mathbf{z} \leq \mathbf{d}_1, \\ & \mathbf{M}_2 \mathbf{z} = \mathbf{d}_2, \\ & \text{and } \mathbf{z} \geq 0, \end{aligned}$$

where  $\mathbf{z}$  is the vector of decision variables, and  $\mathbf{f}^T \mathbf{z}$  is the objective function. Matrix  $\mathbf{M}_1$  and vector  $\mathbf{d}_1$  determine the inequality constraints, whereas matrix  $\mathbf{M}_2$  and vector  $\mathbf{d}_2$  determine the equality constraints. The accurate models derived before are not all immediately applicable for LP as such, and require some adjusting. The various constraints and the used objective function are presented in functional form for clarity in the following sections.

### 4.1 PEV Battery Constraints

The energy and thermal dynamics of the PEV batteries are determined by Eqs. (3.4), (3.11) and (3.12), which are easily converted into applicable linear equality constraints by simply arranging all the state and decision variables on one side of the equation, and all the known pre-determined time series on the other, yielding



$$\begin{aligned}
 \frac{\nu}{1 - e^{-\nu\Delta t}}(E_{v,t+1} - e^{-\nu\Delta t}E_{v,t}) - \eta_b\eta_c(P_{v,t}^+ + G_{v,t}^+ + \eta_F F_{v,t}^+) \\
 + P_{v,t}^- + G_{v,t}^- + \Psi_{v,t}^\pm = -D_{v,t}^- \quad \forall v, t
 \end{aligned} \tag{4.1}$$

$$\begin{aligned}
 T_{b,v,t+1} - \beta_{11}T_{b,v,t} - \beta_{12}T_{c,v,t} + \frac{\gamma_{12}}{C_c}\Phi_{c,v,t}^\pm \\
 + \frac{\gamma_{11}}{C_b} \left[ \Phi_{b,v,t}^\pm + (1 - \eta_b)(\eta_c(P_{v,t}^+ + G_{v,t}^+) + P_{v,t}^- + G_{v,t}^- + \eta_F\eta_c F_{v,t}^+) \right] \quad \forall v, t \\
 = -\frac{\gamma_{11}}{C_b} [H_{be}T_{e,t} + (1 - \eta_b)D_{v,t}^-] - \frac{\gamma_{12}}{C_c} [H_{ce}T_{e,t} + \Lambda_c I_{sol,t}]
 \end{aligned} \tag{4.2}$$

$$\begin{aligned}
 T_{c,v,t+1} - \beta_{21}T_{b,v,t} - \beta_{22}T_{c,v,t} + \frac{\gamma_{22}}{C_c}\Phi_{c,v,t}^\pm \\
 + \frac{\gamma_{21}}{C_b} \left[ \Phi_{b,v,t}^\pm + (1 - \eta_b)(\eta_c(P_{v,t}^+ + G_{v,t}^+) + P_{v,t}^- + G_{v,t}^- + \eta_F\eta_c F_{v,t}^+) \right] \quad \forall v, t \\
 = -\frac{\gamma_{21}}{C_b} [H_{be}T_{e,t} + (1 - \eta_b)D_{v,t}^-] - \frac{\gamma_{22}}{C_c} [H_{ce}T_{e,t} + \Lambda_c I_{sol,t}]
 \end{aligned} \tag{4.3}$$

where  $v$  is the index of the vehicle. The additional decision variables  $G_{v,t}^+$  and  $G_{v,t}^-$  correspond to the PEV battery exchanging electricity directly with the utility grid while at work, as opposed to the decision variables  $P_{v,t}^+$  and  $P_{v,t}^-$  that are connected to the home MG.  $G_{v,t}^+$  and  $G_{v,t}^-$  are only used in scenarios where the PEV is considered grid connected both at work and at home, and are required to correctly account for possible costs associated with electricity transmission between the home MG and the workplace PEV charging station.

The next step is to constrain the various state and decision variables according to the PEV and V2G infrastructure we wish to simulate. Naturally the PEV battery can only store a limited amount of energy depending on its capacity, and the BMS and A/C thermal elements have some maximum power draws, resulting in the following constraints

$$SOC_{min}(1 - L_{v,t})E_{max,v,0} \leq E_{v,t} \leq (1 - L_{v,t})E_{max,v,0} \quad \forall v, t \tag{4.4}$$

$$0 \leq \psi_{c,v,t}^+ \leq \psi_{max,c,v}^+ \quad \forall v, t \tag{4.5}$$

$$0 \leq \psi_{c,v,t}^- \leq \psi_{max,c,v}^- \quad \forall v, t \tag{4.6}$$

$$0 \leq \psi_{b,v,t}^+ \leq \psi_{max,b,v}^+ \quad \forall v, t \tag{4.7}$$

$$0 \leq \psi_{b,v,t}^- \leq \psi_{max,b,v}^- \quad \forall v, t \tag{4.8}$$

for every vehicle  $v$ .

The constraints for the battery charging and discharging decision variables, as well as for the cabin temperature state variable, are dependent on whether the PEV is idle or driving. The constraints to enforce the correct operation of the PEV battery and A/C system are formulated as

$$0 \leq P_{v,t}^+ + G_{v,t}^+ \leq g_{v,t} P_{max,v}^\pm \quad \forall v, t \quad (4.9)$$

$$0 \leq P_{v,t}^- + G_{v,t}^- \leq g_{v,t} P_{max,v}^\pm \quad \forall v, t \quad (4.10)$$

$$0 \leq G_{v,t}^+ \leq w_{v,t} P_{max,v}^\pm \quad \forall v, t \quad (4.11)$$

$$0 \leq G_{v,t}^- \leq w_{v,t} P_{max,v}^\pm \quad \forall v, t \quad (4.12)$$

$$0 \leq F_{v,t}^+ \leq h_v F_{max,v}^+ \quad \forall v, t \quad (4.13)$$

$$T_{min,c} \leq T_{c,v,t} \leq T_{max,c}, \quad \text{if } D_{v,t}^- > 0 \quad \forall v, t \quad (4.14)$$

where  $g_{v,t}$  is a binary time series determined by the driving pattern of vehicle  $v$  that tells whether the PEV is currently connected to the grid either at home or at work,  $w_{v,t}$  is a binary time series that tells whether the PEV is grid-connected and at work, and  $h_v$  is a PEV type parameter that determines whether the PEV is a BEV or a PHEV. When the PEV is parked, there are no significant constraints on the cabin temperature, but when the vehicle is driven the A/C system is set to keep the cabin temperatures between a set interval for driver comfort in Eq. 4.14.

The constraints on the battery temperature are slightly more convoluted. Depicting a truly intelligent BMS would require additional binary logic variables to keep track whether the batteries of the PEVs are being charged on each time step, in order to tell when the batteries need to be heated or cooled to their permitted charging temperatures. Even though this can be formulated as a MILP problem, it becomes computationally too demanding for our purposes.

The simplest way to account for the BMS heat demand without binary logic variables is to always keep the batteries in charging temperatures when grid-connected even when it's unnecessary, resulting in

$$\left. \begin{array}{l} T_{min,b} \leq T_{b,v,t} \leq T_{max,b}, \quad \text{if } g_{v,t} = 0 \\ 0^\circ\text{C} \leq T_{b,v,t} \leq T_{max,b}, \quad \text{if } g_{v,t} = 1 \end{array} \right\} \quad \forall v, t \quad (4.15)$$

where  $T_{min,b}$  is the minimum permitted temperature and  $T_{max,b}$  is the maximum permitted temperature of the battery. This unavoidably leads to higher than necessary overall electricity consumption of the BMS, but remains computationally efficient. The ideal BMS behaviour could be calculated based on the solution using its known battery use, which would allow us to quantify the energy wasted in needlessly keeping the battery

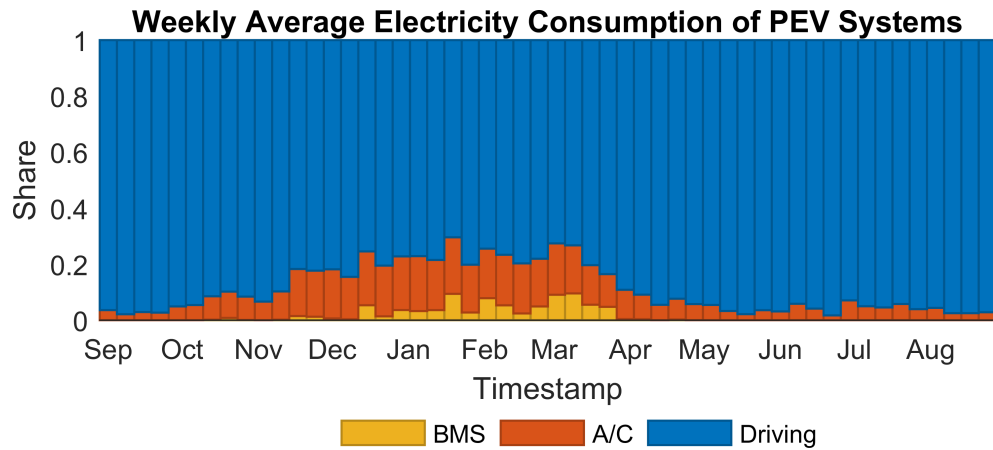


**Figure 4.1.** Shares of the electricity consumption of the different PEV systems calculated from the mean electricity consumptions of 10 simulated *Nissan Leafs*. The BMS is only required in winter when ambient temperatures are too cold for charging, and the results are fairly independent of the PEV model.

in charging temperatures. However, even the overestimated BMS only accounts for only a small portion of the total electricity consumption of the PEV, which can be seen from Figure 4.1. The BMS represents around a percent of the yearly total electricity consumed by the PEV, so any error made remains largely insignificant.

Another approach attempted was to iterate the optimization and update the battery temperature constraints between iterations based on the battery usage of the previous solution. This way the logical binary variables are avoided, as the temperature constraints are predetermined and not dependent on the decision variables, preserving linearity while allowing the battery temperatures to deviate from the desired operating temperatures when the battery is not used. Iterating the temperature constraints ultimately leads to better energy consumption of the BMS than the set temperature range solution, but it never seems to reach convergence with multiple PEVs. This is most likely caused by the optimizer alternating between which PEV battery to use in which situation, depending on which battery has the least strict temperature constraints. This results in the battery use and the operating temperatures never fully coinciding. The number of iterations needed to reach meaningful improvements over the simple set temperature range is also quite large, significantly increasing the computational load.

#### *Battery Capacity Loss*

As can be seen from Eq. (3.18) the battery capacity loss due to usage is non-linear, and thus cannot be explicitly implemented into a linear model. Fortunately, the capacity loss is rather small, and ultimately doesn't have

a major impact on the dynamics of the system as a whole. This allows us to account for it approximately by iterating the optimization problem and updating the battery capacity constraints to match the previous battery usage between iterations.

This isn't a perfect solution, as reaching convergence with more than a few modelled PEVs begins to take excessive amounts of time. However, reasonably small relative capacity excess is reached already with a few iterations, up to around 20 Wh for a few hours at a time. As automotive batteries are not intended to be cycled with 100% DOD to avoid excessive temperature and SOC effects on battery performance and degradation, the minuscule and short-lived overcharges are insignificant.

## 4.2 House HVAC Constraints

The thermal dynamics of the modelled houses with radiator systems are determined by Eqs. (3.25) and (3.26), that are rearranged into applicable equality constraints

$$\begin{aligned} T_{i,h,t+1} - \epsilon_{h,11}T_{i,h,t} - \epsilon_{h,12}T_{f,h,t} + \frac{\zeta_{h,11}}{C_{i,h}}(\alpha_{hp,t}^+P_{h,t}^+ - \alpha_{ac}^-P_{h,t}^-) \\ = -\frac{\zeta_{h,11}}{C_{i,h}}(P_{app,h,t} + \varphi_{ppl,h,t} + \varphi_{sol,h,t} + H_{ie,h}T_{e,t}) \quad \forall h, t \quad (4.16) \\ -\frac{\zeta_{h,12}}{C_{f,h}}(H_{fe,h}T_{e,t}) \end{aligned}$$

$$\begin{aligned} T_{f,h,t+1} - \epsilon_{h,21}T_{i,h,t} - \epsilon_{h,22}T_{f,h,t} + \frac{\zeta_{h,21}}{C_{i,h}}(\alpha_{hp,t}^+P_{h,t}^+ - \alpha_{ac}^-P_{h,t}^-) \\ = -\frac{\zeta_{h,21}}{C_{i,h}}(P_{app,h,t} + \varphi_{ppl,h,t} + \varphi_{sol,h,t} + H_{ie,h}T_{e,t}) \quad \forall h, t \quad (4.17) \\ -\frac{\zeta_{h,22}}{C_{f,h}}(H_{fe,h}T_{e,t}) \end{aligned}$$

for each house  $h$ . The constraints for the radiant floor heating system are the same, except than in Eq.(4.16)  $P_{h,t}^+$  is multiplied by  $\frac{\zeta_{h,12}}{C_{f,h}}$  instead of  $\frac{\zeta_{h,11}}{C_{i,h}}$ , and in Eq. (4.17)  $P_{h,t}^+$  is multiplied by  $\frac{\zeta_{h,22}}{C_{f,h}}$  instead of  $\frac{\zeta_{h,21}}{C_{i,h}}$ . Again, the temperatures and electric powers are constrained to enforce desired behaviour

$$T_{min,i} \leq T_{i,h,t} \leq T_{max,i} \quad \forall h, t \quad (4.18)$$

$$\left. \begin{aligned} T_{min,f} \leq T_{f,h,t} \leq \min(T_{max,f}, T_{sup,h,t}), \quad \text{if } rfh \\ T_{min,f} \leq T_{f,h,t} \leq T_{max,f}, \quad \text{if } rad \end{aligned} \right\} \quad \forall h, t \quad (4.19)$$

$$0 \leq P_{h,t}^+ \leq P_{max,h,t}^+ - \psi_{dhw,h,t} \quad \forall h, t \quad (4.20)$$

$$0 \leq P_{h,t}^- \leq P_{max,h}^- \quad \forall h, t \quad (4.21)$$

where  $\psi_{dhw,h,t}$  is the electricity consumption of heating the DHW with the heat pump, calculated as

$$\psi_{dhw,h,t} = N_{ppl,h} \frac{\phi_{dhw,t}}{\alpha_{dhw}^+}, \quad \forall h, t \quad (4.22)$$

where  $N_{ppl,h}$  is the number of residents in house  $h$  and  $\alpha_{dhw}^+$  is the heat pump COP when heating DHW. The floor node temperatures are constrained according to thermal comfort standards [73].

In Eq. (4.19) when using radiant floor heating  $rfh$  we also restrict the floor node temperature from exceeding the floor heating system supply temperature, in order to prevent the optimizer from heating the floor node to higher than supply temperatures. Unfortunately, this may lead to some excess cooling demand if the supply temperature suddenly drops below floor temperature or the floor node temperature naturally rises above the supply temperature due to changes in ambient temperature. In both cases the constraint would now force the HVAC system to cool the floor node accordingly, but fortunately the temperature constraints of the interior node seem to keep the floor node temperatures low enough even during hot summer days. Even if such excess cooling were to be necessary at times, the modelled cooling system is extremely energy efficient, and would only result in an insignificantly small increase in energy consumption.

Introducing thermal energy storage in the form of hot water storage tanks into the model was attempted, but explicitly modelling the dependency between the heat pump COP and the temperature of the hot water storage tank proved infeasible due to non-linearity and non-convexity issues. Additional attempts with iterating the optimization and updating the storage temperatures, and fixing the storage temperature to the radiator supply temperatures encountered a problem where the heat pump would fully charge the thermal energy storage during the time step with the best COP, violating the second law of thermodynamics during said step. Fixing the COP at a constant value would make the storage tank behave correctly, but would result in wasteful use of energy due to non-optimal use of the heat pump. Ultimately modelling the thermal energy storage was abandoned in favour of correctly modelling the COP of the heat pump in the hydronic heating system. The DHW tank would run into similar problems with the heat pump COP if the temperature of the tank was allowed to vary between the temperatures 50–60°C set in legislation.

### 4.3 Microgrid Power Balance and Objective Functions

So far each modelled PEV and household has not been interconnected in any way. In order to form the desired MG with RE generation, we enforce yet another equality constraint

$$\begin{aligned} \sum_v [P_{v,t}^+ - \eta_b \eta_c P_{v,t}^-] + \sum_h [P_{h,t}^+ + P_{h,t}^-] + G_{s,t} - G_{b,t} \\ = \sum_h [P_{app,h,t} + \psi_{dhw,h,t}] - P_{sol,t} \end{aligned} \quad \forall t \quad (4.23)$$

where  $G_{s,t}$  and  $G_{b,t}$  are the amounts of power sold to and bought from the main electrical grid respectively, and  $P_{sol,t}$  is the PV generation in the MG.

The grid connection variables are constrained according to

$$0 \leq G_{s,t} \leq G_{max}, \quad \forall t \quad (4.24)$$

$$0 \leq G_{b,t} \leq G_{max}, \quad \forall t \quad (4.25)$$

where  $G_{max}$  is the maximum power capacity of the connection between the MG and the utility grid. This value is scaled based on the number of modelled households  $N_h$  in the MG as

$$G_{max} = 24 N_h \text{ kW}. \quad (4.26)$$

Eq. (4.26) is based on an assumption that each house has three 35 A main fuses and phase voltage of 230 V.

It is worth noting that the PEV grid trading decision variables  $G_{v,t}^+$  and  $G_{v,t}^-$  don't appear in Eq. (4.23), as their main function is to distinguish between electricity transferred from the home MG and electricity traded directly while at work. This means that in case the PEVs are considered grid-connected even at the workplace, only the home MG connected charging and discharging terms  $P_{v,t}^+$  and  $P_{v,t}^-$  can be made subject to the possible transmission fees.

With the hourly time scale of the overall model we essentially have to assume that the modelled MG has hourly net-metering, even though hourly net-metering isn't actually used in Sweden. However, hourly net-metering is currently in use in Denmark, and under consideration in Finland as a way to support RE generation. [84]

The objective function used in this work is a total cost minimizing function

$$\begin{aligned} f_{cost} = \sum_t \left[ \sum_v [p_{r,t} G_{v,t}^+ - p_{m,t} \eta_c \eta_b G_{v,t}^- + p_{F,t} F_{v,t}^+ + p_f w_{v,t} (P_{v,t}^+ + \eta_c \eta_b P_{v,t}^-)] \right. \\ \left. + p_{r,t} G_{b,t} - p_{m,t} G_{s,t} \right], \end{aligned} \quad (4.27)$$

where  $p_{F,t}$  is the  $\frac{\text{€}}{\text{Wh}}$  price of fuel. The transmission fees  $p_f$  only apply to power transfer between the MG and the PEV when the PEV is at work, hence the multiplication by  $w_{v,t}$ .

Another objective function that was considered minimized the total amount of electricity bought into the modelled MG, which indirectly encouraged the MG to utilize its local PV generation to its fullest. However this objective function was found to be a little too zealous, as it occasionally utilized the temperatures of the PEV cabin and battery as extremely inefficient energy storages for excess PV. While the bought electricity minimizing objective function technically resulted in slightly increased self-sufficiency of the MG, this often came at a significant extra cost caused by the lost income from sold excess PV generation.

The cost-optimized scheduling of the PEVs and the HVAC systems is compared against a scenario, where the energy consumptions of the PEVs and HVAC systems are optimized separately without any grid interconnections. The resulting baseline represents an equally sophisticated system, except lacking any V2G or DSM capabilities able to take advantage of the real-time pricing.

The baseline PEV charging schedule is calculated by minimizing the usage of the battery

$$f_{PEV} = \sum_t \sum_v [10(F_{v,t}^+ + G_{v,t}^+ + G_{v,t}^-) + P_{v,t}^+ + P_{v,t}^- - 0.1E_{v,t}], \quad (4.28)$$

with an incentive factor of  $-0.1$  for keeping the batteries as full as possible and a penalty factor of  $10$  for fuel usage and direct trading between the PEV and the market. The exact values of the incentive and penalty factors are arbitrary, as long as they place the most weight on the fuel  $F_{v,t}^+$  and direct grid exchange  $G_{v,t}^\pm$ , and the least weight on the energy stored inside the battery  $E_{v,t}$ . The PEV baseline optimization with Eq. (4.28) only uses the PEV constraints in Eqs. (4.1)–(4.15), resulting in each PEV scheduling its charging solely according to its driving pattern. This results in the PEV baseline using as little electricity and fuel as possible to get through the year, while fully charging their batteries as soon as possible after connecting to the grid. The V2G discharge  $P_{v,t}^-$  yields no benefits for the PEV, but is included in Eq. (4.28) for numerical reasons. Since Eq. (4.28) doesn't consider costs and the direct trading terms  $G_{v,t}^+$  and  $G_{v,t}^-$  are penalized, the PEV does all its power transfers through the MG. However, accounting for the correct transmission and direct trading can be done after determining the baseline schedule.

The baseline HVAC system schedule is calculated by minimizing its electricity consumption

$$f_{HVAC} = \sum_t \sum_h [P_{h,t}^+ + P_{h,t}^-], \quad (4.29)$$

while keeping the temperatures within permissible limits, as constrained by Eqs. (4.16)–(4.21). As with the PEVs, this minimizes the amount of electricity used to manage the temperatures inside the houses.

The baseline used in this work is rather tough in the sense that it uses very little energy for the required PEV and HVAC operations, thus making most changes consume more energy than the baseline. However, comparing the V2G and SHLC capable system to anything less efficient would yield seemingly better results partly due to increased energy efficiency, making it harder to quantify the benefits gained solely from the cost-optimal scheduling of the system.



## 5. Results and Discussion

The constructed optimal MG energy management problem was formulated using *MATLAB R2015a*, and solved with *IBM ILOG CPLEX Optimization Studio 12.4*. The optimizations are performed on a single desktop computer with an *Intel Xeon CPU E3-1230 v3* processor and 16 GB of RAM. The largest single optimization sets included 10 households each with their own PEV within the modelled residential MG, and took up to between 15-20 minutes to solve for the modelled year spanning from 2005-9-1 00:00 to 2006-8-31 23:00.

A single optimization sequence consists of first optimizing the baseline PEV and space heating behaviour, then optimizing the full MG energy management problem, and finally optimizing the MG energy management problem by dispatching only the PEVs and only the space heating loads respectively. All the optimizations including PEVs are also iterated a few times in order to sufficiently account for the battery degradation.

It is worth noting that the cost of battery degradation isn't included in the cost optimization due to the non-linear nature of the battery ageing process. Also, in order to correctly estimate the cost of the extra battery degradation caused by V2G discharge, we first have to consider the battery degradation caused by normal PEV use. Hence the costs of battery degradation must be calculated and accounted for separately from the optimization results, and will be discussed separately from the other results.

First, we calculate the cost-optimal scheduling of the individual households, and then proceed to examine how increasing the number of households and amount of PV generation in the modelled MG affects the results. Lastly, we examine whether workplace charging and V2G are worthwhile compared to smart home charging, when accounting for additional electricity transfer fees and costs of battery degradation.

## 5.1 Model Validation

The following sections analyse the validity of the PEV and HVAC models by comparing initial results to those obtained in literature.

### *PEV Model Analysis*

Even though each modelled PEV is technically identical and their driving habits are the same, the generated driving patterns vary considerably, between 18,000 and 20,000 km per PEV per year when using average *stage* distances from the *RES 2005–2006* statistics. This value is high compared to the average Swedish value around 12,000–13,000 km per car per year [85]. However, this value is calculated based on Swedish road traffic statistics, and includes vehicles that are not used regularly for commuting. Since most of the electricity consumed by the PEVs is used for driving, this variance in the total distance driven also affects the yearly electricity consumption of the PEVs.

The driving consumption is affected by the ambient temperatures via the cabin A/C. For the *Nissan Leaf* the average driving electricity consumption is around  $142 \frac{\text{Wh}}{\text{km}}$  over the year, which represents a 13% increase over the UDDS 23°C A/C systems off consumption of  $125 \frac{\text{Wh}}{\text{km}}$  [47]. In [40] this increase in yearly average driving consumption in the comparably cold climate of Minneapolis was found to be around 24%. However, this was calculated for cabin A/C set to 22°C, whereas we use a minimum cabin temperature of 16°C instead. By running our simulation at 22°C minimum cabin temperature, the increase in yearly average driving consumption for the *2013 Nissan Leaf* increases by around 20%, similar to the result in [40]. Experimental data suggests that the driving consumption at  $-7^\circ\text{C}$  could however be as much as 40–120% larger than the no-A/C driving consumption [48]. Our model results in maximum driving consumption increase of around 50–70% for the *Nissan Leaf*, depending on the used minimum cabin temperature, which is reasonable considering the relatively long time step of one hour used in this work. For the *Chevrolet Volt* the increase in average yearly driving consumption is around 11% and the increase in maximum driving consumption is around 81%, whereas for the hypothetical high-end BEV the corresponding values are 10% and 39% respectively.

Figure 5.1 presents two examples on the thermal dynamics of the modelled PEVs, and illustrates the problem associated with the length of the hourly time step. Due to the nature of the thermal model in Eqs. (3.11)

and (3.12), each action affects the temperature on the following time step. This can be seen in Figure 5.1 as the sharp drops in cabin temperature after steps where the cabin is cooled, or as the rise in battery temperature after the PEV is driven. In reality, these effects would take place immediately when cooling or driving begins, but due to the chosen time step the effect is now delayed to the following hour. This delay in the dynamics is the main reason the ageing model in Eq. (3.18) averages the battery temperature over two subsequent steps, in an attempt to account for the changing battery temperature. This delay affects the *Chevrolet Volt* more due to the faster thermal dynamics of the smaller battery, and might have a significant effect on its battery degradation. Increasing the time resolution of the optimization would alleviate this problem, but would require more accurate weather and driving pattern data.

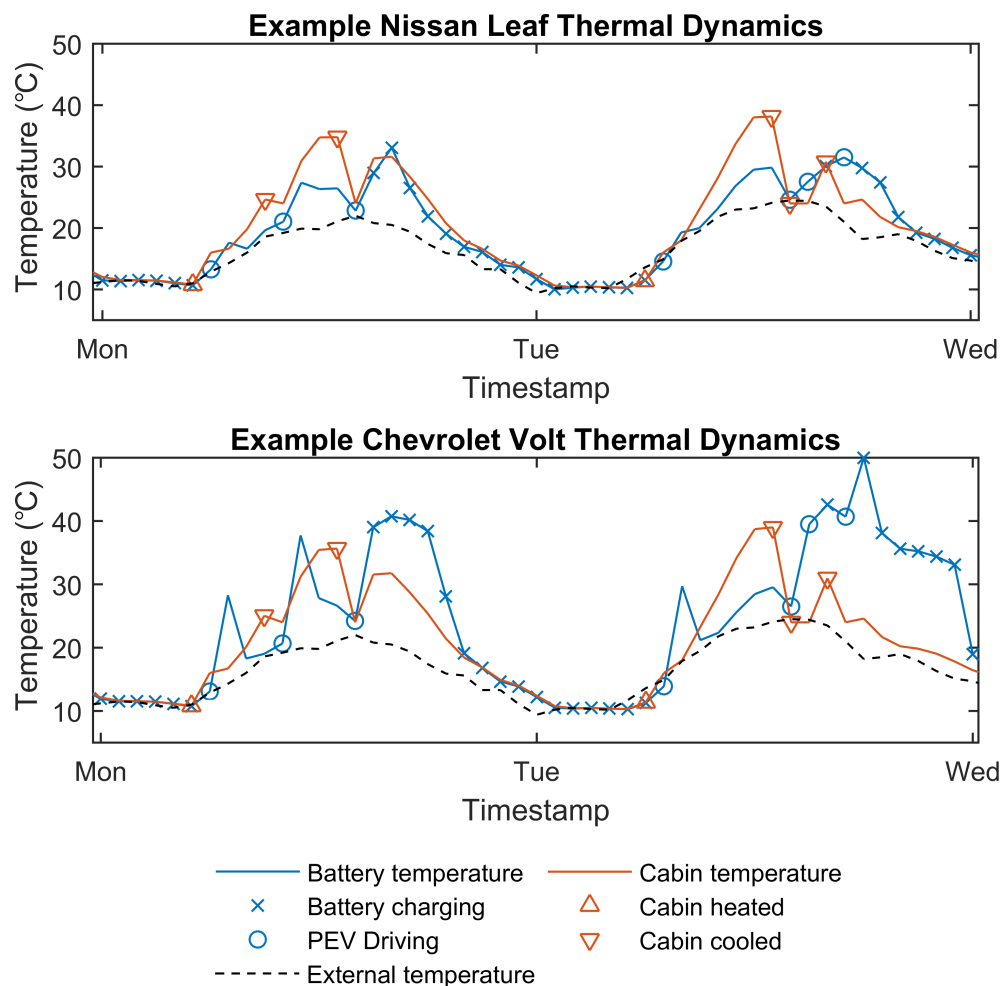


**Figure 5.1.** Examples of the thermal dynamics of the modelled PEVs in early September 2005 with the same driving pattern. The changes in the battery temperature of the *Chevrolet Volt* are much larger and faster than those in the *Nissan Leaf* due to the reduced thermal mass of the smaller battery system. The cabin temperatures rise well above the external temperatures during the day due to solar radiation.

### *House Model Analysis*

The yearly electricity consumption of the appliances and lighting in the modelled houses varies between around 2.3–5.1 MWh, averaging around 4.7 MWh per year. Similarly, the yearly heating demand of the modelled houses varies by quite a bit between around 12.0–21.1 MWh. However, the heating demands per m<sup>2</sup> of the different houses are more similar, varying between around 86.0–105.5  $\frac{\text{kWh}}{\text{m}^2}$  per year, averaging at around 93.0  $\frac{\text{kWh}}{\text{m}^2}$  per year. The corresponding value for the *TABULA* reference house with similar insulation is 93.7  $\frac{\text{kWh}}{\text{m}^2}$  per year, so it seems the space heating model performs adequately. The electricity consumption of the HVAC equipment depends on the system, as the floor heating system achieves an average ground-source heat pump COP of around 4.94 over the year, whereas the radiator heating system only achieves an average COP of 4.37. The floor heating system has a slightly higher yearly heating demand than the radiator heating system due to the fact that it has to heat the floor slab in addition to the house interior, but the floor heating system ends up requiring around 13% less electricity due to the improved heat pump COP achieved with the lower supply temperatures.

The modelled energy demand of DHW is around 814 kWh per person per year, which corresponds well enough with 781 kWh per person per year found in literature [77]. Since the modelled houses have different numbers of inhabitants and the DHW is heated using the heat pump, the yearly electricity consumed by heating the DHW varies between 0.6–1.4 MWh, averaging around 0.7 MWh per year.

### *Overall Performance*

As a whole the model performs well, and attempts to match consumption with local PV generation to minimize the cost of electricity. Figure 5.2 presents two examples of the effect the optimization has on the power balance in a MG with 70 kW<sub>p</sub>, during both summer and winter. During summer the modelled MG is almost capable of meeting all of its electricity demand with local PV generation, with considerable excess PV generation still sold to the market. During winter the local PV generation rarely exceeds electricity consumption, but the optimized solution can be seen shifting consumption from afternoon and evening peak hours to the cheaper early morning hours. During winter the tendency of the cost optimal solution to charge all PEVs simultaneously during the cheapest hours of the early morning is also seen from the peaking of the consumption.

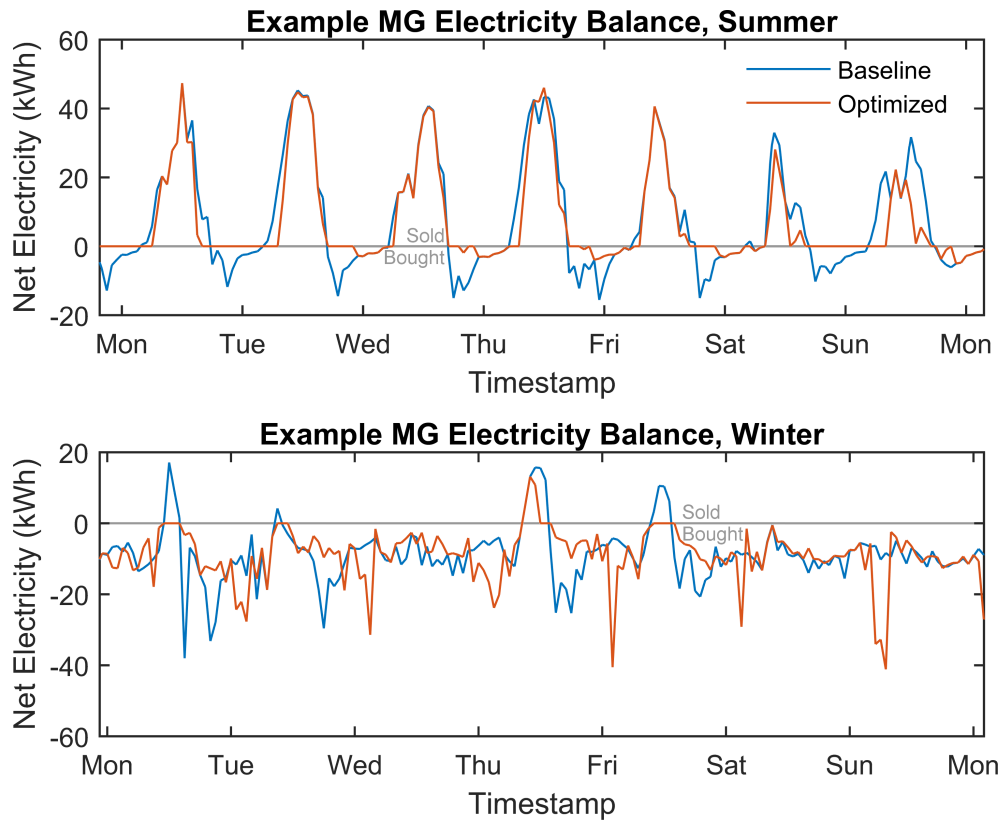


**Figure 5.2.** Examples of the electricity balance in a 5 household MG with *Nissan Leafs* and radiant floor heating systems. The modelled MG has 70 kW<sub>p</sub> of PV generation capacity, matching the yearly electricity consumption of the MG during the modelled year.

By performing the optimization with either the PEVs or the space heating load locked to the baseline behaviour, we can compare the benefits of the individual technologies. It seems that the PEVs offer significantly larger flexibility to the MG, with yearly savings of around €100 (15%) per household with the *Chevrolet Volts*, around €150 (24%) per household with the *Nissan Leafs*, and around €250 (35%) per household with the hypothetical high-end BEVs. By itself the SHLC achieves yearly savings of around €20 (3%) per household with radiator heating systems, around €40 (6%) per household with floor heating systems with a 8 cm thick floor slab, and around €60 (9%) per household with floor heating systems with a 12 cm thick floor slab, referred to as *improved floor heating* for short. These results are calculated from results for a MG with 5 households, with around 70–75 kW<sub>p</sub> of PV generation, enough to match the yearly electricity consumption of the modelled MG including the PEVs.

Compared to the values found in literature [12, 13, 14] ranging from 5–46% savings in heating costs, the results of the separate SHLC optimization might seem low at first. However, our model doesn't include any active thermal storage elements and the results account for costs for the

whole household including the PEVs and appliances, reducing the relative impact of the SHLC. As for the PEVs-only optimization, daily electricity cost savings up to €0.52 were reported in [30] with a PEV comparable to the *Chevrolet Volt* in battery capacity, whereas our initial results vary between €0.27–0.68 depending on the modelled PEV. These results are quite similar considering the optimization in [30] only spanned a single day in Spanish summer climate.

The better flexibility offered by the PEVs is not simply caused by bigger energy storage capacities, but also the fact that the batteries are electricity storages, as opposed to the thermal energy storage capacity offered by the building thermal mass. The flexibility offered by the thermal mass all but vanishes during summer, when there is little heating demand, and the cooling demand is supplied by extremely energy efficient ground source free cooling systems as modelled in this work. By contrast, electricity is still required by the PEVs, household appliances, and lighting. However, currently the PEVs have unrealistic advantage caused by the perfect forecasting of the driving patterns, and their flexibility might be drastically reduced under uncertainty. Naturally the SHLC would suffer from weather and internal heat gain uncertainties as well, but their impact on the HVAC system flexibility would remain comparatively small.

## 5.2 Individual Households

First off, we optimize each of the modelled houses individually in order to determine the benefit to an individual single-family household. Each house is modelled with enough PV generation to account for its yearly electricity demand including the PEV, implying peak power capacities of around 17 kW<sub>p</sub>, 13 kW<sub>p</sub>, 14 kW<sub>p</sub>, 15 kW<sub>p</sub>, and 14 kW<sub>p</sub> for houses 1 through 5 respectively, depending slightly on the modelled PEV and HVAC system. The PEVs are also only considered grid-connected when at home.

As can be seen from Figure 5.3, the modelled houses are rather different from each other, even though the PEV and the HVAC equipment are modelled as identical for each house. The savings in total yearly costs range from around €120 per year for the *Chevrolet Volt* and radiator heating system to around €280 per year for the hypothetical high-end BEV and improved floor heating. The baseline costs for the *Nissan Leaf* scenarios are the cheapest for each house mostly due to the good energy efficiency of the

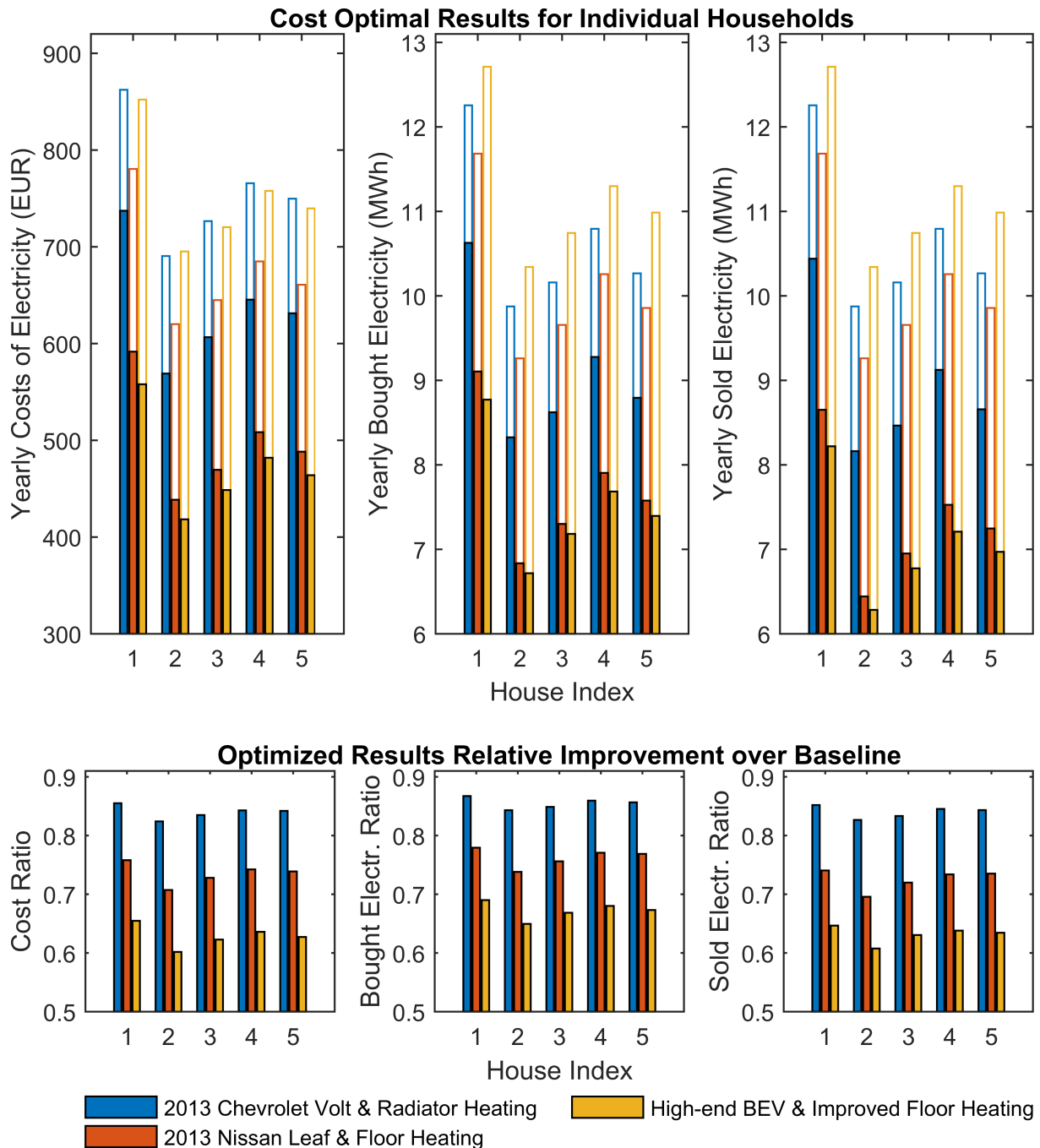


**Figure 5.3.** Cost optimized yearly costs, as well as yearly bought and sold electricity for each of the modelled households, baseline results indicated by the white bars. The *Ratios* in the figures below are calculated by dividing the optimized result by the baseline result. The households are modelled with enough PV generation to account for their yearly electricity demand including the modelled PEVs.

*Nissan Leaf*, but the flexibility offered by the larger battery capacity in the high-end BEV scenario is able to reduce the costs below those of even the optimized *Nissan Leaf*. The *Chevrolet Volt* scenario baselines are about as costly as the high-end BEV baselines depending somewhat on the driving pattern, but perform the worst post-optimization due to limited storage capacity. For individual households, the adoption of V2G and SHLC

seem to result in yearly total electricity cost savings of around €118–125 (14–18%) for PHEVs and radiator heating systems, around €172–188 (24–30%) for BEVs and floor heating systems, and around €275–294 (35–40%) for hypothetical high-end BEVs and heavy floor heating systems. It should be noted that the yearly electricity costs weren't high to begin with due to the large amount of PV and energy efficient baseline.

As expected, the larger battery capacity of the BEVs allows the houses to better utilize the local PV production, resulting in around 23–26% reduction in bought and around 26–31% reduction in sold electricity for the *Nissan Leaf* scenario, and around 31–35% and 36–40% reductions for bought and sold electricity respectively for the high-end BEV scenario. The yearly values vary slightly ( $\approx \pm 2\%$ ) depending on the used driving pattern, but there are no significant changes to the results of the optimization.

### 5.3 Microgrid Size

An interesting question is whether it is worthwhile to aggregate multiple households and PEVs into a larger centrally managed MG. Naturally such a MG would require co-operation from the residents, a cost division scheme that would distribute the aggregated costs between the collaborators according to their participation, as well as infrastructure to exchange the information necessary in the optimization between the households and the MG central management system.

Looking at the measured household results in Figure 5.4a it seems like the relative benefits gained from aggregating multiple households into a large MG are rather unclear. Clearly houses 1 and 2 perform better together than they would on their own, decreasing the cost, as well as sold and bought electricity ratios by around 2–5 pp depending on the modelled PEV and HVAC systems as well as the driving patterns. Adding house 3 still often seems to lead into noticeable decrease in the ratios, although only by around 1–2 pp. However, adding houses 4 and 5 into the MG doesn't seem to yield any additional relative benefits. Since the modelled households have quite different yearly electricity consumptions and driving patterns, it makes comparing the grid sizes quite difficult.

In order to better compare the benefits from MGs of various sizes, the electricity consumption of each household and PEV are normalized. For the household electricity consumption, the experimental *SEA* residential electricity consumption time series are scaled so that the total yearly elec-



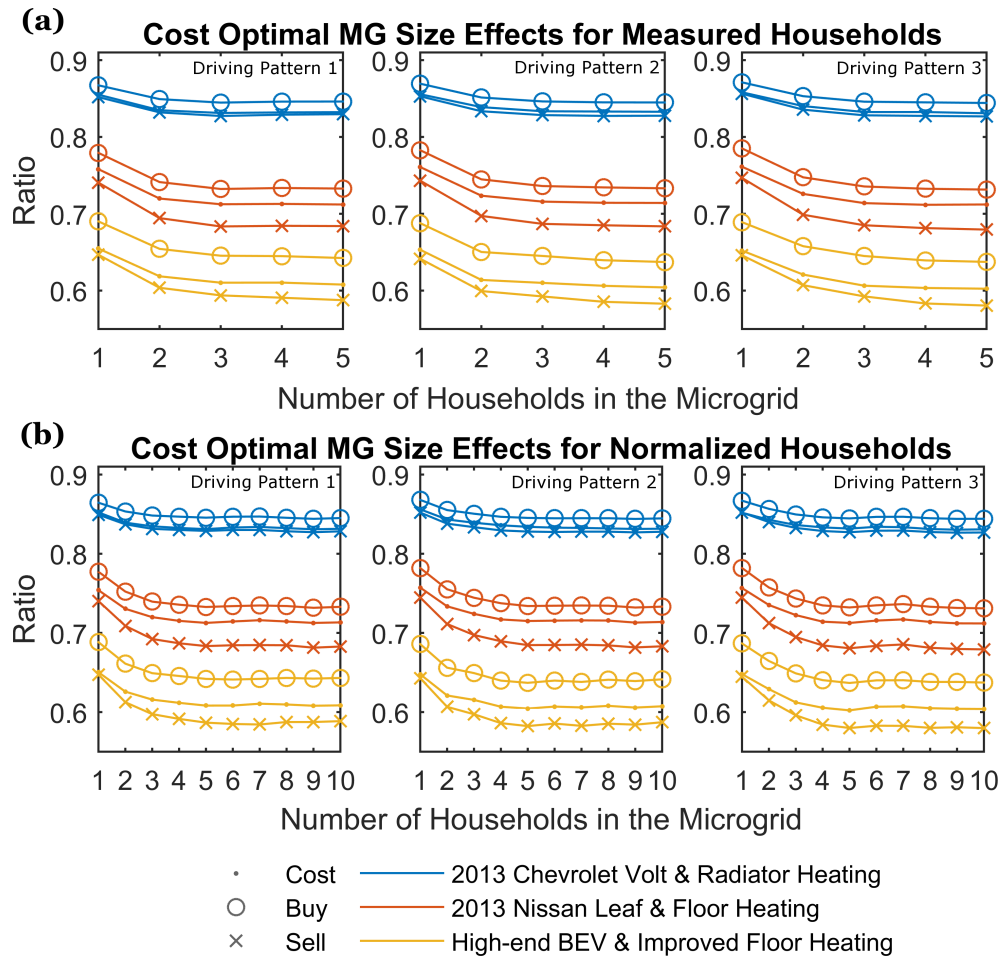


**Figure 5.4.** The relative benefits of various MG sizes for the different PEV and HVAC system types, for both the measured and normalized households, using 3 different driving profiles. Houses are added to the MG in the order of their indexing, and the MG is modelled to have enough PV generation to account for its yearly electricity consumption including the PEVs. The effect of the randomness in the driving profiles can be seen from the small variations in the ratios after the maximum benefits have been reached at 5 households and above, and changing the order the houses are added to the MG has a similar effect.

tricity consumption of each household equals the mean yearly consumption of the experimental data of the detached houses used in this work, at around  $4.7 \frac{\text{MWh}}{\text{a}}$ . Similarly, the yearly HVAC consumption of the households is made approximately equal by modelling each house with identical dimensions, estimated based on the mean floor area of the *SEA* data houses used in this work presented in Table 3.4. Each household is also set to have the same number of residents in order to equalize the internal heat gains from inhabitants, as well as DHW electricity consumption, set to the average value of 2.7 inhabitants per household. Even though each house is identical, the yearly electricity consumption of the HVAC system varies a bit due to the different internal heat gains from the appliances. Although the yearly electricity consumption of the appliances in

each household is normalized, the waste heat from the appliances is more valuable for the HVAC system when the external temperature is low.

The household electricity consumption normalization also allows us to extend the modelled MG from 5 to 10 households by using *SEA* electricity consumption data from 5 apartments measured at roughly the same time in 2005–2006. Naturally, since apartments and detached houses generally have different sets of electric appliances, these 5 extra electric consumption profiles are slightly different in shape from the house profiles. Nonetheless, they are considered sufficiently similar for our purposes.

The electricity consumption of the modelled PEVs is normalized by scaling the length of the individual trips of each car, so that the total yearly distance driven equals the mean value of the statistics-based driving generator of around 18,900 km per PEV per year. As with the house HVAC systems, the total electricity consumption of the PEV cabin A/C systems and BMS thermal elements still vary between PEVs due to different driving patterns.

The normalized MG results also presented in Figure 5.4b provide a slightly clearer picture on the benefits of aggregating multiple households into a single centrally managed MG. As with the measured case, the step from a lone household to a pair of co-operating households yields the largest relative benefits, around 1–5 pp reduction in the cost, as well as sold and bought electricity ratios. With the normalized households however, the ratios continue to decrease until the MG has around 4–5 co-operating households, after which any additional households don't seem to noticeably increase the relative benefits. Determining the most cost-efficient MG size would require detailed information about the sort of neighbourhood in question, as well as the type of extra infrastructure required for the communications and DSM optimization.

It is rather interesting that the relative benefits gained from increasing the size of the MG seem to stagnate around 4–5 households regardless of the modelled PEVs and HVAC systems. Naturally one would need more co-operating PHEVs than BEVs to reach similar absolute benefits, but apparently the relative benefits are more dependent on the properties of the individual co-operators than their number. However, this could change if uncertainty were to be introduced into the model, as increasing the number of modelled PEVs would probably "smooth" the uncertainty associated with their driving profiles.

## 5.4 Photovoltaic Generation

Another aspect of interest is the role of the PV generation in the MG, and the effect its amount has on the performance of the V2G and building MPC systems. Here we measure the amount of PV generation as a fraction of the total yearly PV production divided by the total yearly electricity consumption of the modelled MG, called *PV fraction* in Figure 5.5. The PV fractions of 0.5, 1.0, and 1.5 correspond to around 7–8 kW<sub>p</sub>, 14–15 kW<sub>p</sub>, and 21–23 kW<sub>p</sub> of installed solar capacity per household respectively, depending slightly on the modelled PEVs and HVAC systems. The effect of the MG size was found to be independent of the PV fraction as well, meaning that the MG size of 5 households should yield the best benefits per household.

From Figure 5.5 it is apparent that without any PV generation the flexibility offered by the V2G and SHLC technologies can only achieve yearly cost savings of around €20–50 (2–4%) per household, and since no consumption can be curtailed and the baseline is already energy efficient the amount of bought electricity cannot be decreased. In this case the cost savings are achieved by shifting consumption from expensive hours into cheaper ones. As the PV fraction is increased, the PEVs and HVAC systems begin shifting their consumption into hours with excess PV generation, which can be seen in the decreased amount of electricity traded with the utility grid of the optimized results. Naturally the costs are decreased further as more PV generation is added into the grid, with the optimal high-end BEV scenario almost turning a profit with a PV fraction of 1.5. With a PV fraction of 2.0, all scenarios except the PHEV baseline already turn a profit during the year. The value of the extra flexibility offered by the high-end BEV scenario can be seen when comparing the costs and bought electricity amounts between the 0.5 and 1.0 PV fraction scenarios, as the high-end BEV scenario overtakes the *Nissan Leaf* one as the cheapest alternative.

In [31], yearly total costs were reduced from €1800 to €630 (–65%) after installing around 5 kW<sub>p</sub> of solar capacity. According to our results, such an improvement seems to require at least 14–15 kW<sub>p</sub> of solar capacity per household, but this is without the residential CHP system, extra 7.8 kWh electricity storage, and appliance level DSM. In the author’s experience appliance level DSM doesn’t have a large impact on the yearly costs, but such extra gains from CHP and an extra battery seem rather incredible.

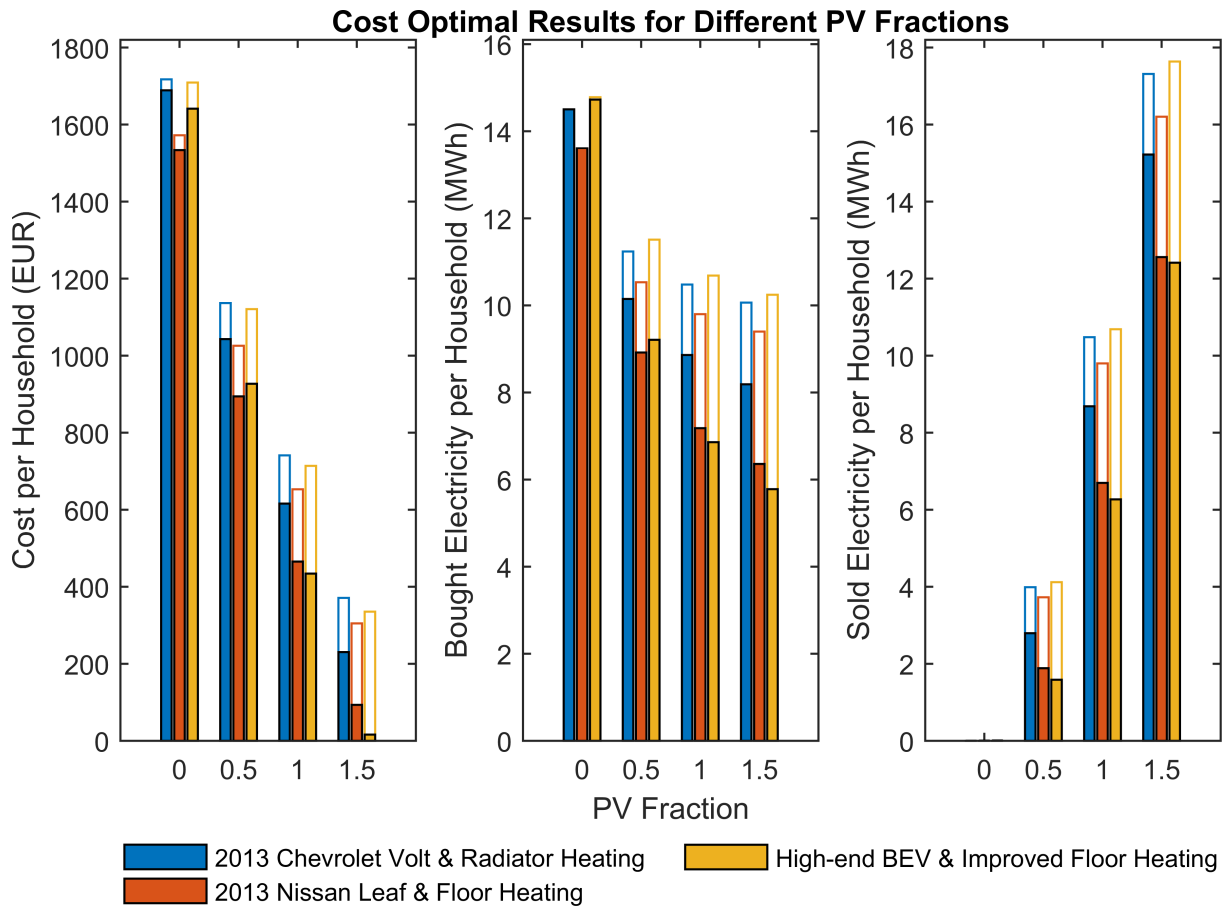
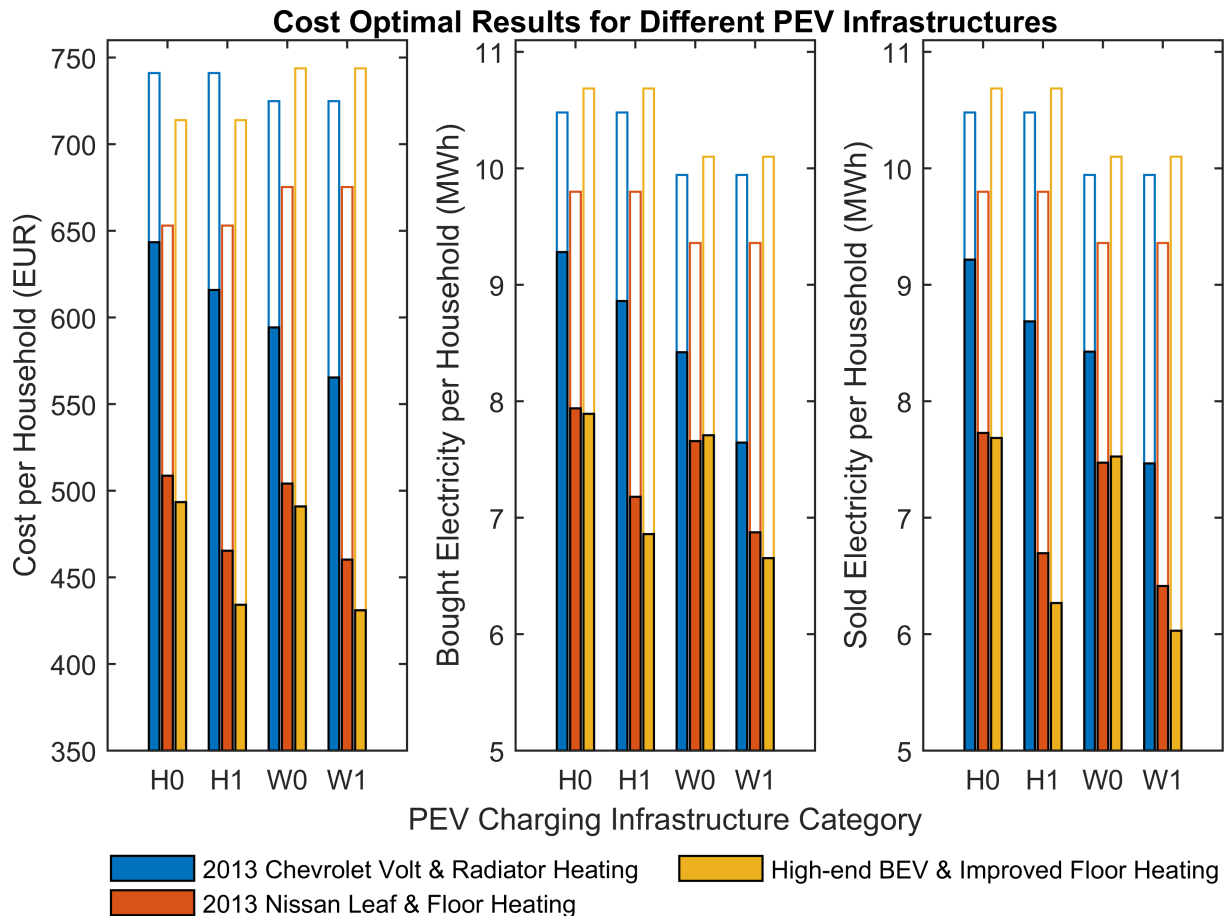


**Figure 5.5.** Cost optimized results for a MG with 5 normalized households with different amounts of PV generation, depicted here as a fraction of the yearly electricity consumption called *PV fraction*. The white bars indicate the baseline results.

## 5.5 PEV Infrastructure

Finally, we examine the effects of the PEV charging infrastructure on the MG. One interesting question is whether V2G provides any significant benefits over only smart charging when accounting for the extra battery wear. Another point of interest is how much the PEV flexibility can be improved by introducing PEV charging infrastructure to the workplace, as the PEVs typically spend the most solar intensive hours of the day away from home at work. In order for this to increase the flexibility of the modelled MG however, transferring the RE generation from the MG to the workplace over the utility grid needs to be possible. This would allow the PEVs to utilize the PV generation of the home MG when at work at a cost, possibly yielding additional savings.

As can be seen from Figure 5.6, the *2013 Chevrolet Volt* PHEV gains the most benefits from being able to charge its batteries at work, thus reducing its fuel consumption. The yearly fuel consumption of the PHEVs is reduced from around 35 l to 2 l (−94%) when charging at the workplace is



H0	Grid connected only at home, smart charging without V2G
H1	Grid connected only at home, full V2G capability
W0	Grid connected at home and at work, smart charging without V2G
W1	Grid connected at home and at work, full V2G capability

**Figure 5.6.** Cost optimized results for a MG with 5 normalized households and a PV fraction of 1.0. Baseline results indicated by the white bars.

allowed, as the PHEV battery is large enough for the individual trips, but not for multiple trips in succession. The baseline PHEV behaviour seems to be able manage mostly on electricity, as for comparison a pure ICE vehicle would need around 1200 l of fuel to make it through the year. Since electricity is generally cheaper than fuel in series PHEV mode, charging at the workplace reduces PHEV operating costs.

The increase in the BEV baseline costs when charging at the workplace is caused by the transmission costs, and the fact that the PEV baseline isn't price-conscious. This means that every time the BEV goes to work or makes a trip while at work, it either buys electricity from the market or transfers excess PV from the home MG at a cost to charge itself full again. It seems that the modelled transmission fee is large enough to make it uneconomical to use most excess PV this way, as the benefits

barely increase. Removing the transmission fees completely would drop the yearly costs per household by around €20–70 in the workplace charging scenarios.

Comparing the V2G and smart charging only scenarios, the costs per household decrease by around €20–50 per year by using V2G. The additional battery wear in the V2G capable scenarios is around 0.3–0.4% for the high-end BEVs, around 0.4–0.6% for the *Nissan Leaf*, and around 0.3–0.5% for the *Chevrolet Volt*, which amount to capacity losses of around 210–280 Wh, 96–144 Wh, and 50–83 Wh respectively. Estimates on the cost of modern Li-ion EV batteries vary by quite a lot, between around 260–360  $\frac{\text{€}}{\text{kWh}}$  [86], placing the costs of V2G battery wear between around €13–100 per year. For the high-end BEV the costs of the additional battery wear associated with the V2G are larger than the benefits even when using the lowest price estimate for the battery capacity. However, the *Nissan Leaf* and the *Chevrolet Volt* seem to be able to profit from the V2G discharge for up to around €10 per household per year with the lowest battery price estimate.

This is an interesting result, as it suggests that V2G could be economically feasible for distributed energy storage purposes even with concurrent battery technology and without income from grid regulatory services, contrary to [42]. As the LP model is currently incapable of explicitly taking the costs associated with battery wear into account during the optimization, this most likely results in excessive V2G use, particularly with the modelled high-end BEV. If the costs of battery degradation could be included in the LP formulation, for example by using a linear approximation of the battery ageing process, both the *Nissan Leaf* and the high-end BEV would probably limit their V2G discharge to times when the monetary benefits exceed the battery wear costs. For the *Chevrolet Volt* such benefits would remain significantly smaller though, as typically PHEV batteries are 30–50% more expensive due to higher requirements on battery power density [86].

## 6. Summary and Conclusions

In this work, we assess the economical benefits of V2G and SHLC for residential consumers with local PV generation. A SHLC-capable house energy model is constructed based on residential electricity consumption data by *SEA* [43] and *TABULA* national building typologies [56], coupled to a PEV model constructed using travel survey statistics [4] and experimental PEV data [47, 48]. The PEV model accounts for the thermal behaviour of the vehicle battery and cabin [40], as well as battery degradation [55]. The houses, the PEVs, and the PV generation are linked through LP methodology, and the cost optimal energy management is then solved using *IBM ILOG CPLEX Optimization Studio 12.4*. The optimizations are performed for a MG consisting of 1–10 detached houses located in Norrköping, Sweden (58.58°N 16.15°E), for a full year from 2005-9-1 00:00 to 2006-8-31 23:00 on a hourly time scale. The different PEVs modelled in this work include the *2013 Chevrolet Volt*, *2013 Nissan Leaf*, and a hypothetical high-end BEV based mainly on *2013 Tesla Model S*. The modelled house HVAC systems include hydronic radiator and floor heating systems, with ground source heat pumps and free cooling systems.

The PEV model was found to be consistent with existing literature [40], with 10–13% increase in average electricity consumption due to the cabin A/C systems in the cold climate of Sweden. The electricity consumption of the PEV battery thermal management was found to be largely insignificant, even though the used model exaggerates its consumption. However, due to the relative roughness of the hourly time step, the PEV cabin and battery thermal dynamics are slower than they would in reality, which could have an impact on the modelled battery degradation. The HVAC model of the detached houses also performed adequately, with the average heating demands per m<sup>2</sup> as well as the DHW energy demand corresponding well to existing literature [56, 77].

The overall MG model performed as expected, shifting the PEV and HVAC loads to match excess local PV generation, as well as other hours with comparably cheap electricity. During summer the modelled MG with 70 kW<sub>p</sub> occasionally managed to function without buying any electricity for a few days at a time, thanks to the local PV generation and the storage capacity offered by the PEVs and the building thermal mass. The flexibility offered by the PEVs was estimated to be around 4–5 times more valuable for the modelled MG than the flexibility offered by the SHLC, excluding the additional costs associated with battery wear.

For individual households, yearly cost savings of around €120–290 (14–40%) were achieved compared to the established baseline, depending on the modelled PEVs and HVAC systems. The households were modelled with enough PV generation to match their yearly electricity consumption including the PEV and an energy efficient baseline, so the yearly costs in this case weren't high to begin with. The benefits of increasing the MG size by aggregating multiple households into a single centrally optimized entity were found to saturate at around 4–5 households, only yielding an additional 5 pp decrease in yearly costs per household over the single household case. This could change if uncertainty were to be introduced to the driving patterns, as increasing the number of PEVs would probably smooth the combined uncertainty of the individual PEVs.

Changing the amount of PV generation in the modelled MG demonstrated that the relative savings achievable with intelligent energy management increase along with the amount of PV generation. Without any PV generation the storage capacity offered by the PEVs and the building thermal mass can only take advantage of the real-time-pricing, reducing the achieved savings to around €20–50 (2–4%) per year. In an attempt to further increase the benefits of self-consuming local PV generation, a system where a PEV owner could transfer excess PV from the home MG to a workplace charging station at a cost was also studied. While the *Chevrolet Volt* achieved significant savings due to reduced fuel consumption thanks to workplace charging, the *Nissan Leaf* and the high-end BEV didn't achieve significant savings under the modelled transmission fees.

V2G was found to result in additional yearly cost savings compared to smart charging-only scenarios, but after accounting for the additional battery wear the benefits become dubious. However, the results suggest that V2G could be economically feasible as a distributed energy storage resource even with concurrent battery technology, contrary to [42]. How-



ever, it is clear that the degradation costs cannot be ignored in the V2G optimization, as otherwise the V2G might be used excessively.

While the LP energy management model constructed in this work succeeds in finding the exact global cost-optimal V2G and SHLC scheduling in a small residential MG and yields some interesting results, it still leaves a few things to be desired. As the current model operates on perfect knowledge of weather, appliance electricity consumption, activities of the inhabitants, electricity prices, and PEV driving patterns, the results of this work essentially represent the best possible savings achievable under the modelled conditions. If this type of energy management were to be applied in real life, these would have to be forecast or otherwise determined ahead of time, likely to include significant errors. According to [27] the uncertainty associated with PEV availability is especially important for this type of energy management, making it an important aspect for possible future research. Since the model is currently linear, robust optimization seems like a promising approach [87]. However, the nature and magnitude of the uncertainty associated with the PEV driving patterns requires further contemplation, since the driving pattern forecasts are mainly dependent on the driver. How accurate the forecast trip schedule is, are all forecast trips driven, and when does the PEV know for certain are all questions that would need to be answered.

Even though thermal energy storage elements, couldn't be successfully included into the model in this work, they are worth considering. DHW storage tanks and other hot water storage tanks could offer the HVAC systems considerable extra flexibility, provided they could be modelled properly within the LP framework. For instance, some sort of plug-flow model might be possible with the temperature dependent COP of the ground source heat pump. Phase-change materials could also be considered as possible thermal energy storage elements.

Another important research aspect would be to include the costs associated with battery degradation into the LP model, as the results indicate that these costs clearly cannot be ignored in V2G energy management optimization. As battery ageing is an inherently non-linear process, it cannot be explicitly included in a linear model. However, taking advantage of the fact that battery degradation is a rather slow process, it might be possible to derive a reasonable approximation based on the battery degradation iterations already performed in this model. This way the V2G could restrict its output only to times when it is truly economical, and should

always be able to outperform smart charging-only scenarios even when battery costs are accounted for.

Finally, the thermal and battery ageing modelling of the PEVs could be further refined. The hourly time step is too long for realistic modelling of the PEV cabin and batteries, as explained in Section 5.1. Shortening the time step to at least 10 minutes could significantly improve the thermal modelling and by extension the degradation, as well as the accuracy of the grid interactions, reducing our dependency on the assumed hourly net-metering. Unfortunately this would require more accurate weather and behavioural data, as well as significantly increasing the computational load. However if the MG size truly has such a limited impact on the benefits of V2G and SHLC, a single household could perhaps be reasonably optimized for an entire year with 10-minute time steps. *Calendar ageing* of the batteries can be included as well to further improve the accuracy of the batter degradation model, but whether it would be affected differently by V2G and smart charging remains dubious.

# Bibliography

- [1] IEA. *Key World Energy Statistics 2014*. OECD Publishing, 2014.
- [2] J. Klimstra. *Power Supply Challenges - Solutions for Integrating Renewables*. Wärtsilä Finland Oy, 2014.
- [3] P. D. Lund, J. Lindgren, J. Mikkola, and J. Salpakari. Review of energy system flexibility measures to enable high levels of variable renewable electricity. *Renewable and Sustainable Energy Reviews*, 45:785–807, 2015.
- [4] L. Abramowski and A. Holmström. Res 2005-2006, the national travel survey. Technical report, Swedish Institute for Transport and Communications Analysis, Oct 2007.
- [5] D. B. Richardson. Electric vehicles and the electric grid: A review of modeling approaches, Impacts, and renewable energy integration. *Renewable and Sustainable Energy Reviews*, 19:247–254, 2013.
- [6] T. S. Ustun, C. Ozansoy, and A. Zayegh. Recent developments in microgrids and example cases around the world - A review. *Renewable and Sustainable Energy Reviews*, 15(8):4030–4041, 2011.
- [7] S. Prívará, J. Cigler, Z. Váňa, F. Oldewurtel, C. Sagerschnig, and E. Žáčková. Building modeling as a crucial part for building predictive control. *Energy and Buildings*, 56:8–22, 2013.
- [8] H. Hao, Y. Lin, A. S. Kowli, P. Barooah, and S. Meyn. Ancillary Service to the grid through control of fans in commercial Building HVAC systems. *IEEE Transactions on Smart Grid*, 5(4):2066–2074, 2014.
- [9] M. Sullivan, J. Bode, B. Kellow, S. Woehleke, and J. Eto. Using residential AC load control in grid operations: PG&E’s ancillary service pilot. *IEEE Transactions on Smart Grid*, 4(2):1162–1170, 2013.
- [10] J. Ma, S. J. Qin, and T. Salsbury. Application of economic MPC to the energy and demand minimization of a commercial building. *Journal of Process Control*, 24(8):1282–1291, 2014.
- [11] M. Avcı, M. Erkoç, A. Rahmani, and S. Asfour. Model predictive HVAC load control in buildings using real-time electricity pricing. *Energy and Buildings*, 60:199–209, 2013.
- [12] R. Halvgaard, N. K. Poulsen, H. Madsen, and J. B. Jorgensen. Economic Model Predictive Control for building climate control in a Smart Grid. *2012 IEEE PES Innovative Smart Grid Technologies (ISGT)*, pages 1–6, 2012.

- [13] B. Favre and B. Peuportier. Application of dynamic programming to study load shifting in buildings. *Energy and Buildings*, 82:57–64, 2014.
- [14] M. Ali, J. Jokisalo, K. Siren, and M. Lehtonen. Combining the demand response of direct electric space heating and partial thermal storage using LP optimization. *Electric Power Systems Research*, 106:160–167, 2014.
- [15] D. Vanhoudt, D. Geysen, B. Claessens, F. Leemans, L. Jespers, and J. Van Bael. An actively controlled residential heat pump: Potential on peak shaving and maximization of self-consumption of renewable energy. *Renewable Energy*, 63:531–543, 2014.
- [16] S. Rahman and G. B. Shrestha. Investigation into the impact of electric vehicle load on the electric utility distribution system. *IEEE Transactions on Power Delivery*, 8(2):591–597, 1993.
- [17] K. Clement-Nyns, E. Haesen, and J. Driesen. The impact of Charging plug-in hybrid electric vehicles on a residential distribution grid. *IEEE Transactions on Power Systems*, 25(1):371–380, 2010.
- [18] P. Finn, C. Fitzpatrick, and D. Connolly. Demand side management of electric car charging: Benefits for consumer and grid. *Energy*, 42(1):358–363, 2012.
- [19] K. Mets, T. Verschueren, W. Haerick, C. Davelder, and F. De Turck. Optimizing smart energy control strategies for plug-in hybrid electric vehicle charging. *2010 IEEE/IFIP Network Operations and Management Symposium Workshops*, pages 293–299, 2010.
- [20] B. Lunz, Z. Yan, and D. U. Gerschler, J. B. and Sauer. Influence of plug-in hybrid electric vehicle charging strategies on charging and battery degradation costs. *Energy Policy*, 46:511–519, 2012.
- [21] M. Yilmaz and P. T. Krein. Review of the impact of vehicle-to-grid technologies on distribution systems and utility interfaces. *IEEE Transactions on Power Electronics*, 28(12):5673–5689, 2013.
- [22] W. Kempton and S. E. Letendre. Electric vehicles as a new power source for electric utilities. *Transportation Research Part D: Transport and Environment*, 2(3):157–175, 1997.
- [23] H. Lund and W. Kempton. Integration of renewable energy into the transport and electricity sectors through V2G. *Energy Policy*, 36(9):3578–3587, 2008.
- [24] P. Denholm, M. Kuss, and R. M. Margolis. Co-benefits of large scale plug-in hybrid electric vehicle and solar PV deployment. *Journal of Power Sources*, 236:350–356, 2013.
- [25] E. Sortomme and M. A. El-Sharkawi. Optimal scheduling of vehicle-to-grid energy and ancillary services. *IEEE Transactions on Smart Grid*, 3(1):351–359, 2012.
- [26] J. A. Peças Lopes, S. A. Polenz, C. L. Moreira, and R. Cherkaoui. Identification of control and management strategies for LV unbalanced microgrids with plugged-in electric vehicles. *Electric Power Systems Research*, 80(8):898–906, 2010.

- [27] C. Battistelli, L. Baringo, and A. J. Conejo. Optimal energy management of small electric energy systems including V2G facilities and renewable energy sources. *Electric Power Systems Research*, 92:50–59, 2012.
- [28] M. Honarmand, A. Zakariazadeh, and S. Jadid. Integrated scheduling of renewable generation and electric vehicles parking lot in a smart microgrid. *Energy Conversion and Management*, 86:745–755, 2014.
- [29] W. Su, J. Wang, and J. Roh. Stochastic energy scheduling in microgrids with intermittent renewable energy resources. *IEEE Transactions on Smart Grid*, 5(4):1876–1883, 2014.
- [30] L. Igualada, C. Corchero, M. Cruz-Zambrano, and F. J. Heredia. Optimal energy management for a residential microgrid including a vehicle-to-grid system. *IEEE Transactions on Smart Grid*, 5(4):2163–2172, 2014.
- [31] M. Rastegar and M. Fotuhi-Firuzabad. Load management in a residential energy hub with renewable distributed energy resources. *Energy and Buildings*, 107:234–242, 2015.
- [32] Z. Rao and S. Wang. A review of power battery thermal energy management. *Renewable and Sustainable Energy Reviews*, 15(9):4554–4571, 2011.
- [33] L. Lu, X. Han, J. Li, J. Hua, and M. Ouyang. A review on the key issues for lithium-ion battery management in electric vehicles. *Journal of Power Sources*, 226:272–288, 2013.
- [34] A. Barré, B. Deguilhem, S. Grolleau, M. Gérard, F. Suard, and D. Riu. A review on lithium-ion battery ageing mechanisms and estimations for automotive applications. *Journal of Power Sources*, 241:680–689, 2013.
- [35] D. A. Corrigan and A. Masias. Batteries for electric and hybrid vehicles. In T. Reddy, editor, *Linden’s Handbook of Batteries, 4th Edition*. McGraw-Hill Education, 2010.
- [36] Nissan Motor Co., Ltd. *Nissan Leaf 2013 Owner’s Manual*, 2012.
- [37] Mitsubishi Motors Corp. *Mitsubishi I-MiEV 2012 Owner’s Manual*, 2011.
- [38] J. Fan and S. Tan. Studies on Charging Lithium-Ion Cells at Low Temperatures. *Journal of The Electrochemical Society*, 153(6):A1081, 2006.
- [39] K. Smith, M. Earleywine, E. Wood, J. Neubauer, and A. Pesaran. Comparison of Plug-In Hybrid Electric Vehicle Battery Life Across Geographies and Drive Cycles. *SAE International*, 01(June 2015), 2012.
- [40] J. Neubauer and E. Wood. Thru-life impacts of driver aggression, climate, cabin thermal management, and battery thermal management on battery electric vehicle utility. *Journal of Power Sources*, 259:262–275, 2014.
- [41] C. Zhou, K. Qian, M. Allan, and W. Zhou. Modeling of the cost of EV battery wear due to V2G application in power systems. *IEEE Transactions on Energy Conversion*, 26(4):1041–1050, 2011.
- [42] S. Han, S. Han, and H. Aki. A practical battery wear model for electric vehicle charging applications. *Applied Energy*, 113:1100–1108, 2014.

- [43] J. P. Zimmermann. End-use metering campaign in 400 households in Sweden - assessment of the potential electricity savings. Technical report, Swedish Energy Agency, Sep 2009.
- [44] J. Widén. Improved photovoltaic self-consumption with appliance scheduling in 200 single-family buildings. *Applied Energy*, 126:199–212, 2014.
- [45] J. Smart. Advanced vehicle testing activity – cold weather on-road testing of a 2012 Chevrolet Volt. Technical report, Idaho National Laboratory, Dec 2014.
- [46] General Motors LLC. *2013 Chevrolet Volt Owner Manual*, 2012.
- [47] Idaho National Laboratory and U.S. Department of Energy. Advanced vehicle testing activity database. <http://avt.inl.gov/index.shtml>.
- [48] Argonne National Laboratory and U.S. Department of Energy. Downloadable dynamometer database. <http://www.anl.gov/energy-systems/group/downloadable-dynamometer-database>.
- [49] Y. Ji, Y. Zhang, and C.-Y. Wang. Li-Ion Cell Operation at Low Temperatures. *Journal of the Electrochemical Society*, 160(4):A636–A649, 2013.
- [50] S. Santhanagopalan, K. Smith, J. Neubauer, G.H. Kim, A. Pesaran, and M. Keyser. *Design and Analysis of Large Lithium-Ion Battery Systems*. Artech House Publishers, 2014.
- [51] Tesla Motors, Inc. *Tesla Model S Owner's Manual*, 2012. <http://www.teslamotors.com/sites/default/files/Model-S-Owners-Manual.pdf> (Retrieved 12.8.2015).
- [52] U.S. Department of Energy. Where the energy goes: Hybrids. <https://www.fueleconomy.gov/feg/atv-hev.shtml> (Retrieved 22.7.2015).
- [53] Inc. Tesla Motors. Tesla motors sverige website, model s. [http://www.teslamotors.com/sv\\_SE/models-charging#/basics](http://www.teslamotors.com/sv_SE/models-charging#/basics) (Retrieved 12.8.2015, in Swedish).
- [54] A. A. Pesaran. Battery Thermal Management in EVs and HEVs : Issues and Solutions. *Advanced Automotive Battery Conference*, page 10, 2001.
- [55] A. Cordoba-Arenas, S. Onori, Y. Guezennec, and G. Rizzoni. Capacity and power fade cycle-life model for plug-in hybrid electric vehicle lithium-ion battery cells containing blended spinel and layered-oxide positive electrodes. *Journal of Power Sources*, 278(0):473 – 483, 2015.
- [56] Intelligence Energy Europe Project TABULA. National building typologies database. <http://episcope.eu/building-typology/>.
- [57] S. Burke. Crawl spaces in wood framed single family dwellings in Sweden: unwanted yet popular. *Structural Survey*, 25(1):51–60, 2007.
- [58] K. K. Andersen, H. Madsen, and L. H. Hansen. Modelling the heat dynamics of a building using stochastic differential equations. *Energy and Buildings*, 31(1):13–24, 2000.
- [59] L. Lundgren and K. Rydenstram. The Swedish time use survey 1990/91. Technical report, Statistics Sweden, Oct 1992.

- [60] Refrigerating American Society of Heating and Inc. Air-Conditioning Engineers. 2009 ashrae handbook fundamentals inch-pound edition, 2009.
- [61] M. Molén. The swedish time use survey 2010/11. Technical report, Statistics Sweden, Jun 2012.
- [62] P. D. Lund and H. Faninger-Lund. Integration of building and solar energy systems into one predesign tool. Presented at EUROSUN '98, Sep 1998.
- [63] J. Vinha. *RIL 255-1-2014 Rakennusfysiikka 1, Rakennusfysikaalinen suunnittelu ja tutkimukset (Building physics 1, building physics design and research)*. Suomen Rakennusinsinöörien Liitto, RIL ry, 2014. (in Finnish).
- [64] O. Seppänen. *Rakennusten lämmitys (Heating of Buildings)*. Suomen LVI-yhdistysten liitto, 2001. (in Finnish).
- [65] L. Holm and G. Essunger. *SBN 1975 utgava 3, Svensk Byggnorm (Swedish Building Regulations 1975 3rd Edition)*. Statens Planverk, Feb 1978. (in Swedish).
- [66] T. Cholewa, M. Rosiński, Z. Spik, M. R. Dudzińska, and A. Siuta-Olcha. On the heat transfer coefficients between heated/cooled radiant floor and room. *Energy and Buildings*, 66:599–606, 2013.
- [67] K. Sirén. Jäähdytysjärjestelmien energialaskentaopas (energy calculation guide for cooling systems). Technical report, Finnish Ministry of the Environment, Sep 2011. (in Finnish).
- [68] P. Ljunggren J. Wollerstrand and P-O. Johansson. Optimal reglering av radiatorsystem (optimal regulation of radiator systems). Technical report, Svensk Fjärrvärme AB, 2007. (in Swedish).
- [69] NIBE Energy Systems AB. *NIBE F1155 Ground Source Heat Pump Product Leaflet*, 2014.
- [70] R. Wikstén. *Lämpövoimaprocessit (Thermodynamic Processes)*, in Finnish. Helsinki University Press, 4th edition, 2009.
- [71] H. F. Sullivan. Principles of vapour compression heat pumps. In J. Berghmans, editor, *Heat Pump Fundamentals*, pages 14–33. Martinus Nijhoff Publishers, The Hague, 1983.
- [72] N. Leppäharju. Kalliolämmön hyödyntämiseen vaikuttavat geofysikaaliset ja geologiset tekijät (geophysical and geological factors affecting the use of bedrock heat). master's thesis, University of Oulu, Apr 2008. (in Finnish).
- [73] B. W. Olesen. Radiant floor heating in theory and practice. *ASHRAE Journal*, 44(7):19–26, 2002.
- [74] A. Larsson. Boverkets författningssamling, bfs2006:12, bbr12 (statute book by boverket), Apr 2006. (in Swedish).
- [75] J. Widén, M. Lundh, I. Vassileva, E. Dahlquist, K. Ellegård, and E. Wäckelgård. Constructing load profiles for household electricity and hot water from time-use data-Modelling approach and validation. *Energy and Buildings*, 41(7):753–768, 2009.

- [76] R. Nordman Å. Wahlström and U. Pettersson. Mätning av kall- och varmvatten i tio hushåll (measuring cold and hot water in ten households). Technical report, The Swedish Energy Agency, Apr 2008. (in Swedish).
- [77] T. Levander and L. Stengård. Mätning av kall- och varmvattenanvändning i 44 hushåll (measuring cold and hot water usage in 44 households). Technical report, The Swedish Energy Agency, Jul 2009. (in Swedish).
- [78] S. Cao, A. Hasan, and K. Sirén. Analysis and solution for renewable energy load matching for a single-family house. *Energy and Buildings*, 65:398–411, 2013.
- [79] Norrköping Vatten och Avfall AB. Water quality reports. <http://www.norrkopingsvattenavfall.se/verksamhet/vatten/vattenkvalitet/> (Retrieved 24.6.2015).
- [80] T. Carlund (SHMI). Private communication, Nov 2014.
- [81] Nord Pool Spot. Website. <http://www.nordpoolspot.com/> (Retrieved 15.7.2014).
- [82] European Energy Commission. Weekly oil bulletin newsletter. <http://ec.europa.eu/energy/en/statistics/weekly-oil-bulletin> (Retrieved 2.6.2015).
- [83] Alternative Fuels Data Center U.S. Department of Energy. Fuel properties comparison chart, Oct 2014. [http://www.afdc.energy.gov/fuels/fuel\\_comparison\\_chart.pdf](http://www.afdc.energy.gov/fuels/fuel_comparison_chart.pdf) (Retrieved 18.6.2015).
- [84] RES LEGAL Europe. Regulations on re generation. <http://www.res-legal.eu/home/> (Retrieved 18.9.2015).
- [85] A. Myhr and T. Sehalic. Fordon 2014 (vehicles 2014). Technical report, Trafikanalys, Mar 2014. [http://trafa.se/PageDocuments/FORDON\\_2014.pdf](http://trafa.se/PageDocuments/FORDON_2014.pdf) (Retrieved 7.8.2015, in Swedish).
- [86] B. Nykvist and M. Nilsson. Rapidly falling costs of battery packs for electric vehicles. *Nature Climate Change*, 5(April):100–103, 2015.
- [87] D. Bertsimas, D. B. Brown, and C. Caramanis. Theory and applications of robust optimization. *SIAM Review*, 53(3):464–501, 2011.



# A. Linear Differential Equation System

Here, we present a detailed solution to a linear differential equation in the form of

$$\frac{d}{dt}\mathbf{x}(t) - \mathbf{A}\mathbf{x}(t) = \mathbf{b},$$

where both  $\mathbf{A} \in \mathbb{R}^2$  and  $\mathbf{b} \in \mathbb{R}^2$  are independent of time  $t$ , and  $\mathbf{A}$  is invertible. First we prove that for an invertible  $\mathbf{A}$ , all matrices  $\mathbf{A}$ ,  $\mathbf{A}^{-1}$  and  $e^{\mathbf{A}t}$  are mutually commutative. Starting from the matrix exponential power series definition

$$e^{\mathbf{X}} = \sum_{k=0}^{\infty} \frac{1}{k!} \mathbf{X}^k,$$

by replacing  $\mathbf{X}$  by  $\mathbf{A}t$ , where  $t \in \mathbb{R}$  we get

$$e^{\mathbf{A}t} = \sum_{k=0}^{\infty} \frac{1}{k!} (\mathbf{A}t)^k = \sum_{k=0}^{\infty} \frac{1}{k!} \mathbf{A}^k t^k.$$

If  $\mathbf{A}$  is invertible, we can write

$$\begin{aligned} e^{\mathbf{A}t} &= \sum_{k=0}^{\infty} \frac{1}{k!} (\mathbf{I}\mathbf{A})^k t^k \\ &= \sum_{k=0}^{\infty} \frac{1}{k!} (\mathbf{A}^{-1}\mathbf{A}\mathbf{A})^k t^k \\ &= \sum_{k=0}^{\infty} \frac{1}{k!} (\mathbf{A}^{-1}\mathbf{A}\mathbf{A})(\mathbf{A}^{-1}\mathbf{A}\mathbf{A}) \dots (\mathbf{A}^{-1}\mathbf{A}\mathbf{A})(\mathbf{A}^{-1}\mathbf{A}\mathbf{A}) t^k \\ &= \sum_{k=0}^{\infty} \frac{1}{k!} \mathbf{A}^{-1}\mathbf{A}(\mathbf{A}\mathbf{A}^{-1})\mathbf{A}(\mathbf{A}\mathbf{A}^{-1}) \dots (\mathbf{A}\mathbf{A}^{-1})\mathbf{A}(\mathbf{A}\mathbf{A}^{-1})\mathbf{A}\mathbf{A} t^k \\ &= \sum_{k=0}^{\infty} \frac{1}{k!} \mathbf{A}^{-1}\mathbf{A}^k \mathbf{A} t^k \\ &= \mathbf{A}^{-1} \left[ \sum_{k=0}^{\infty} \frac{1}{k!} \mathbf{A}^k t^k \right] \mathbf{A} \\ &= \mathbf{A}^{-1} e^{\mathbf{A}t} \mathbf{A} \end{aligned}$$

which can easily be shown to hold true also for

$$e^{\mathbf{A}t} = \mathbf{A}e^{\mathbf{A}t}\mathbf{A}^{-1}$$

simply by multiplying  $\mathbf{A}$  by  $\mathbf{I}$  on the first row from the right instead of the left. It now follows that

$$\begin{aligned}\mathbf{A}e^{\mathbf{A}t} &= \mathbf{A}\mathbf{A}^{-1}e^{\mathbf{A}t}\mathbf{A} = e^{\mathbf{A}t}\mathbf{A}, \text{ and} \\ \mathbf{A}^{-1}e^{\mathbf{A}t} &= \mathbf{A}^{-1}\mathbf{A}e^{\mathbf{A}t}\mathbf{A}^{-1} = e^{\mathbf{A}t}\mathbf{A}^{-1},\end{aligned}$$

thus proving that matrices  $\mathbf{A}$ ,  $\mathbf{A}^{-1}$  and  $e^{\mathbf{A}t}$  are mutually commutative.

Second, we again use the matrix exponential power series definition in order to determine the time derivative

$$\begin{aligned}\frac{d}{dt}e^{\mathbf{A}t} &= \frac{d}{dt} \sum_{k=0}^{\infty} \frac{1}{k!} \mathbf{A}^k t^k \\ &= \sum_{k=0}^{\infty} \frac{1}{k!} \mathbf{A}^k \frac{d}{dt} t^k \\ &= \sum_{k=1}^{\infty} \frac{1}{(k-1)!} \mathbf{A}^k t^{k-1} \\ &= \mathbf{A} \sum_{k=1}^{\infty} \frac{1}{(k-1)!} \mathbf{A}^{k-1} t^{k-1} \\ &= \mathbf{A}e^{\mathbf{A}t},\end{aligned}$$

which is nice and similar to a regular exponential function derivative.

Finally we can solve the original linear differential equation system using the properties proven above. Here, the solution is calculated over an arbitrary time interval  $\Delta t$ , which in the LP modelling corresponds to the time step

$$\begin{array}{l|l}\frac{d}{dt}\mathbf{x}(t) - \mathbf{A}\mathbf{x}(t) = \mathbf{b}, & \left| e^{-\mathbf{A}t}.\right. \\ e^{-\mathbf{A}t} \frac{d}{dt}\mathbf{x}(t) - e^{-\mathbf{A}t}\mathbf{A}\mathbf{x}(t) = e^{-\mathbf{A}t}\mathbf{b}, & \left| e^{-\mathbf{A}t}\mathbf{A} = \mathbf{A}e^{-\mathbf{A}t}\right. \\ \frac{d}{dt} \left( e^{-\mathbf{A}t}\mathbf{x}(t) \right) = e^{-\mathbf{A}t}\mathbf{b}, & \left| \int_t^{t+\Delta t} dt\right. \\ \left( e^{-\mathbf{A}t}\mathbf{x}(t) \right) \Big|_t^{t+\Delta t} = -\mathbf{A}^{-1} \left( e^{-\mathbf{A}t} \right) \Big|_t^{t+\Delta t} \mathbf{b}, & \left| e^{\mathbf{A}(t+\Delta t)}.\right.\end{array}$$

finally resulting in

$$\mathbf{x}(t + \Delta t) - e^{\mathbf{A}\Delta t}\mathbf{x}(t) = -(\mathbf{I} - e^{\mathbf{A}\Delta t})\mathbf{A}^{-1}\mathbf{b}.$$